JBC RESEARCH ARTICLE

Targeting HNRNPA2B1 to overcome chemotherapy resistance in gastric cancer stem cells: Mechanisms and therapeutic potential

Received for publication, July 16, 2024, and in revised form, December 31, 2024 Published, Papers in Press, January 25, 2025,
https://doi.org/10.1016/j.jbc.2025.108234

Miao Yu[1,*,‡], **Bingyuan Fei**[1], **and Songtao Chu**[2,*,‡]

From the [1]*Department of Gastrointestinal colorectal and anal surgery, The Third Bethune Hospital of Jilin University, Changchun, Jilin Province, China;* [2]*Department of Forensic Medicine of Basic Medical College, Beihua University, Jilin, Jilin Province, China*

Reviewed by members of the JBC Editorial Board. Edited by Paul Shapiro

Gastric cancer (GC) remains a significant global health challenge, particularly due to the resistance of gastric cancer stem cells (GCSCs) to chemotherapy. This study investigates the role of heterogeneous nuclear ribonucleoprotein A2/B1 (HNRNPA2B1), a member of the heterogeneous nuclear ribonucleoproteins (hnRNPs), in modulating mitochondrial metabolic reprogramming and contributing to chemoresistance in GCSCs. Through extensive analysis of tumor cancer genome atlas (TCGA) and gene expression omnibus (GEO) datasets, HNRNPA2B1 was identified as a key regulator in GCSCs, correlating with poor prognosis and enhanced resistance to chemoresistance. CRISPR-Cas9 mediated knockout of HNRNPA2B1 in GCSCs led to a significant decrease in mitochondrial function, reduced migration, invasion, and sphere formation abilities, and markedly increased apoptosis. These changes were accompanied by a shift in metabolic activity, evidenced by decreased oxygen consumption and increased extracellular acidification. Our results highlight HNRNPA2B1 as a pivotal factor in sustaining the malignant phenotype of GCSCs and present it as a potential therapeutic target to improve chemotherapy efficacy in GC.

Gastric cancer (GC) is one of the malignancies with a high global mortality rate, often limited in its treatment effectiveness due to drug resistance in gastric cancer stem cells (GCSCs) (1–3). The high mortality rate and the issue of chemotherapy resistance in GC pose substantial challenges to clinical treatment (4–6). In recent years, an increasing number of studies have indicated the significant role of GCSCs in GC, as they possess the ability to self-renew, differentiate into various cell types, and resist the effects of chemotherapy drugs, leading to recurrence and metastasis of GC (7, 8). Therefore, it is of paramount importance to identify and study drug targets in GCSCs and understand their molecular mechanisms and regulatory pathways to advance GC treatment.

Heterogeneous nuclear ribonucleoproteins (hnRNPs) are a class of functionally rich nuclear proteins that exist widely in the nucleus and cytoplasm and play crucial roles in processes such as gene expression regulation, RNA processing, and transport (9–11). In recent years, an increasing number of studies have revealed the important role of hnRNPs in regulating stem cell biology functions, particularly in metabolic reprogramming and chemotherapy resistance formation (12–14). However, the mechanism and regulatory network of hnRNPs in GCSCs remains unclear (15).

Studies have shown that the hnRNP family plays a critical role in transcription and RNA metabolism after binding to mRNA. It regulates various processes, including alternative splicing of pre-mRNA, RNA nuclear transport, translation, and stability control. Dysregulation of hnRNPs contributes to abnormal expression patterns, promoting malignant abilities in cancer cells (16). However, the precise mechanisms influencing GC remain unclear. Therefore, the first step of our study involved bioinformatics analysis to screen candidate genes associated with hnRNPs' regulation of GC.

To further understand the role of HNRNPA2B1, this study employed multiple methods. First, a systematic analysis of GC datasets from the cancer genome atlas (TCGA) and gene expression omnibus (GEO) databases was conducted to screen differentially expressed genes (DEGs) related to hnRNPs, followed by functional enrichment analysis (17–19). Flow cytometry was used to isolate highly pure $CD24^+$ $CD44^+$ GCSCs from MKN-45 and TMK-1 cells, confirming their stemness properties (20). HNRNPA2B1 expression was significantly elevated in these cells. CRISPR-Cas9 technology was used to knock out HNRNPA2B1 in MKN-45 and TMK-1 GCSCs, and experiments were conducted to assess the effects of this knockout on chemotherapy sensitivity, migration, invasion, stemness, and apoptosis. Additionally, a gene rescue experiment was performed to determine if restoring HNRNPA2B1 expression could reverse these phenotypes.

This study aims to explore the mechanism of HNRNPA2B1 in GCSCs and its influence on chemotherapy drug sensitivity, unveiling its potential application value in GC treatment. HNRNPA2B1 may emerge as a new potential target in GC treatment, with the potential to improve the response of GC patients to chemotherapy drugs, enhancing treatment effectiveness. Furthermore, the results of this study also hold

‡ These authors contributed equally to this work.
* For correspondence: Miao Yu, yumiao0305@jlu.edu.cn; Songtao Chu, chusongtao0705@163.com.

guiding significance for understanding the treatment of other tumor types, potentially providing new insights and targets for tumor therapy. By conducting in-depth research on the function of HNRNPA2B1 in GCSCs, we can gain further insights into the pathogenesis of GC, thereby providing new strategies and approaches for personalized treatment of GC.

Results

Bioinformatics analysis identifies three hnRNPs as candidate target genes with differential expression in GC

GC has long been recognized as one of the leading malignancies worldwide. Since 2012, it has ranked fifth in incidence and third in mortality (21, 22). In China, GC accounts for approximately 405,000 new cases and 325,000 deaths, making it the third most prevalent cancer-related fatal disease (23).

Early-stage GC can be cured through surgical resection; however, most patients are diagnosed at an advanced stage, often accompanied by lymph nodes and distant metastases. Chemotherapy is an essential treatment for advanced GC, yet the chemoresistance found in GCSCs frequently limits its efficacy (24). GCSCs in GC possess the ability for self-renewal and multi-lineage differentiation and are considered key contributors to malignant progression, recurrence, and chemoresistance. Therefore, uncovering the mechanisms of chemoresistance in GCSCs within GC cells holds crucial importance for improving GC treatment outcomes (25).

To begin, differential expression analysis was performed on the GC dataset GSE54129. Using the Limma package, a total of 13,670 significant DEGs were identified, including 6964 upregulated DEGs and 6706 downregulated DEGs (Fig. 1*A*). Similarly, differential expression analysis was conducted on the GC dataset GSE5801, resulting in 8868 significant DEGs, including 5172 upregulated DEGs and 3696 downregulated DEGs (Fig. 1*B*). To further refine the selection of meaningful DEGs, the results from both datasets were intersected, yielding 4871 DEGs (Fig. 1*C*).

The DEGs were subjected to gene ontology (GO) functional analysis and Kyoto Encyclopedia of Genes and Genomes (KEGG) pathway analysis. The results of the GO functional analysis (Fig. 1, *D*–*G*) revealed that the DEGs are involved in various biological processes (BP), including biological adhesion, secretion, and cell activation. In terms of cellular components (CC), the DEGs were mainly enriched in secretory granules, respiratory bodies, and vesicular cavities. Regarding molecular functions (MF), they were primarily enriched in oxidoreductase activity, collagen binding, and lipid binding. KEGG pathway analysis indicated that the DEGs participate in pathways such as extracellular matrix-cell communication, fatty acid metabolism, and metabolic pathways.

We retrieved GC-related genes using the GeneCards database, applying a relevance score of ≥10 as the selection criterion, resulting in 2133 genes associated with GC. Among these, we selected the top 10 genes related to hnRNPs. By employing Venn analysis, we ultimately identified three hnRNP target genes (TP53, HNRNPK, and HNRNPA2B1) differentially expressed in GC (Fig. 1*H*). Research has shown that overexpression of hnRNP is associated with poor prognosis in GC patients. These hnRNPs regulate oncogenic signaling pathways in GC cells by directly binding and modulating mRNA stability. Based on this finding, we postulate that these three target genes are involved in the pathogenesis of GC, further strengthening the hypothesis that these genes could serve as potential targets for hnRNP-mediated intervention in the treatment of GC.

Correlation of TP53, HNRNPK, and HNRNPA2B1 expression levels with prognosis in patients with GC

In the TCGA database, a comparison was made between gene expression levels in GC and normal gastric tissues, revealing significantly higher expression levels of TP53, HNRNPK, and HNRNPA2B1 in GC patients (Fig. 2*A*). These findings suggest that alterations in the expression levels of these three candidate target genes may play a crucial role in the progression and worsening of GC and are correlated with the prognosis of GC. By dividing GC patients into high and low-expression gene groups, the Kaplan-Meier survival curve demonstrated that patients with high expression of TP53 and HNRNPA2B1 had lower overall survival (OS), while patients with low expression of HNRNPK had lower OS (Fig. 2*B*).

HNRNPA2B1: A significant diagnostic biomarker in GC

To further identify more meaningful target genes and evaluate their diagnostic efficacy in GC, we employed ROC curves to plot the area under the curve (AUC) in training set GSE54129 and validation set GSE65801 among the three candidate target genes identified from the aforementioned analysis. The results showed that the AUC values of TP53, HNRNPK, and HNRNPA2B1 were all greater than 0.7 in both the training and validation sets. By applying the criterion of an AUC value exceeding 0.7, it can be concluded that these three genes exhibit high diagnostic accuracy, highlighting their potential value in disease state recognition. In the validation set, HNRNPA2B1 had the highest AUC value of 0.790, indicating its superior diagnostic efficacy (Fig. 3, *A* and *B*). Furthermore, a comparison of the expression levels of these three genes between GC tissues and control samples in the validation set revealed a significant upregulation of TP53, HNRNPK, and HNRNPA2B1 in GC tissues (Fig. 3, *C*–*E*).

Considering the above results collectively, HNRNPA2B1 may serve as a significant diagnostic biomarker in GC, whereas the diagnostic efficacy of other biomarkers may be influenced by sample selection and experimental conditions. These findings provide potential biomarker candidates for the molecular diagnosis of GC and may have guiding significance in future clinical diagnostic and therapeutic strategies.

HNRNPA2B1 involvement in mitochondrial metabolic reprogramming in GC

HNRNPA2B1 may play a critical role in the initiation and progression of cancer, particularly in GC (24). To meet the demands of rapid proliferation, cancer cells often alter their energy metabolism through metabolic reprogramming (26).

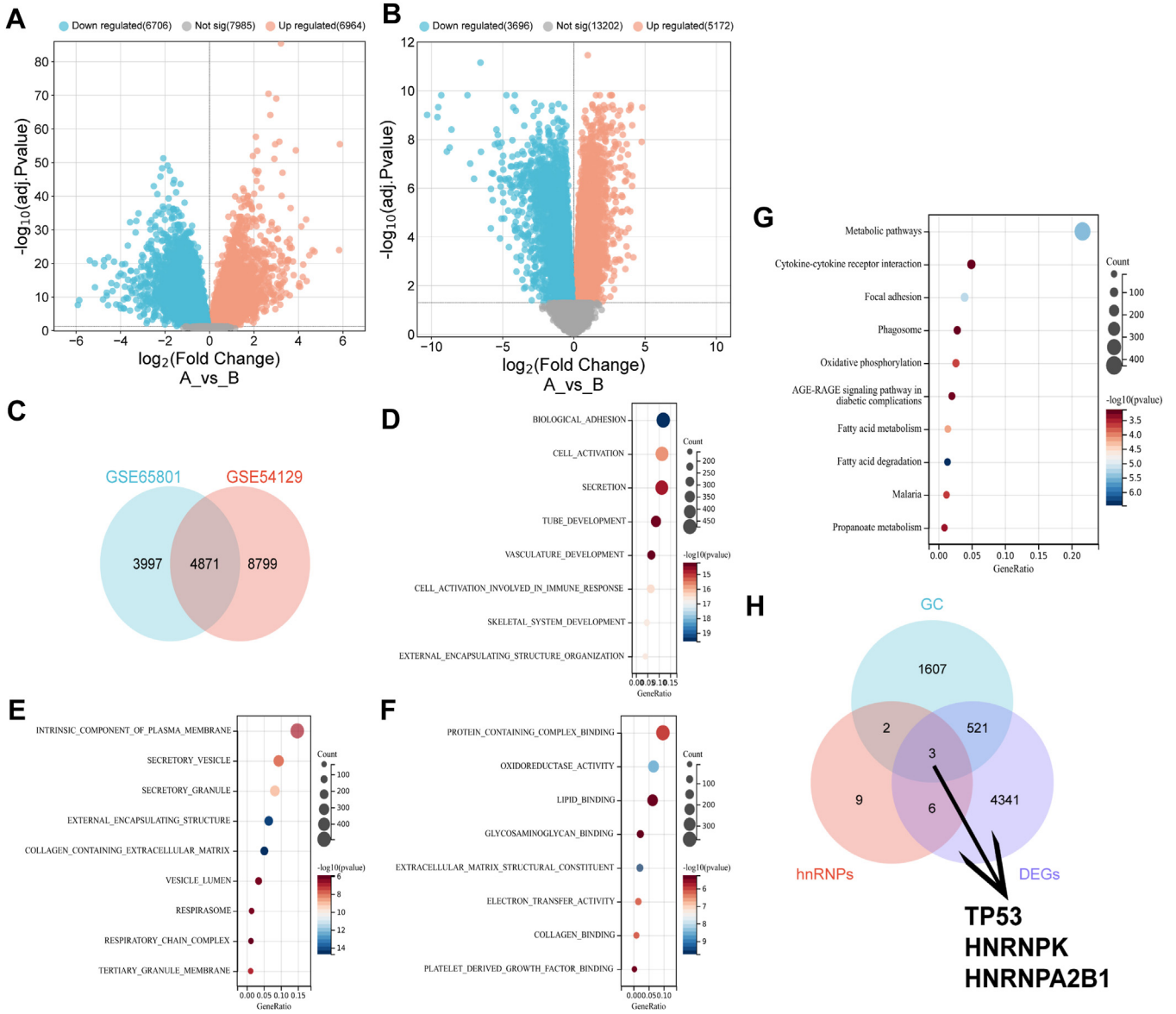

Figure 1. Differential expression of hnRNPs target genes in GC. *A*, volcano plot illustrating the expression of DEGs in the GSE54129 dataset, with *blue* indicating significantly downregulated genes, *red* indicating significantly upregulated genes, and *gray* indicating genes with no significant difference (Control: n = 21; GC: n = 111). *B*, volcano plot showing the expression of DEGs in the GSE5801 dataset (Control: n = 32; GC: n = 32). *C*, intersection of DEGs in the GSE54129 and GSE5801 datasets; *D–F*, bubble plots representing the GO functional analysis of DEGs in GC at the BP, CC, and MF levels, with bubble size indicating the number of selected genes and color representing the enrichment analysis *p*-value; *G*, bubble plot depicting the KEGG pathway enrichment analysis of DEGs in GC. *H*, Venn diagram showing the overlap between DEGs and genes related to GC and hnRNPs identified through the GeneCards database.

HNRNPA2B1 is likely involved in this process by regulating the expression of genes associated with mitochondrial function and energy metabolism. For example, it may influence the expression of genes related to oxidative phosphorylation, glycolysis, or other energy metabolism pathways, thereby promoting the survival and proliferation of cancer cells (27).

To further explore the potential mechanisms of HNRNPA2B1 in GC, we performed a Pearson correlation analysis between HNRNPA2B1 expression levels and the top 10 genes associated with mitochondrial metabolic reprogramming. To ensure accuracy, one outlier sample was excluded from the analysis. Pearson correlation analysis showed a significant negative correlation between HNRNPA2B1 and SLC25A4, and a significant positive correlation with TFAM and SCO2 (Fig. 4, *A–C*). These genes are involved in mitochondrial metabolic reprogramming. SLC25A4 encodes a protein that plays a role in maintaining the balance of the mitochondrial nucleotide pool (28). Mitochondrial transcription factor A (TFAM) is a mitochondrial protein encoded by nuclear genes and transported from the cytoplasm to the mitochondria. TFAM is essential for the maintenance, expression, and delivery of mitochondrial DNA (mtDNA) and can regulate mtDNA replication and transcription (29). SCO2 mainly affects cellular energy metabolism by regulating electron transfer in the mitochondrial respiratory chain (30). These results suggest that HNRNPA2B1 may be involved in

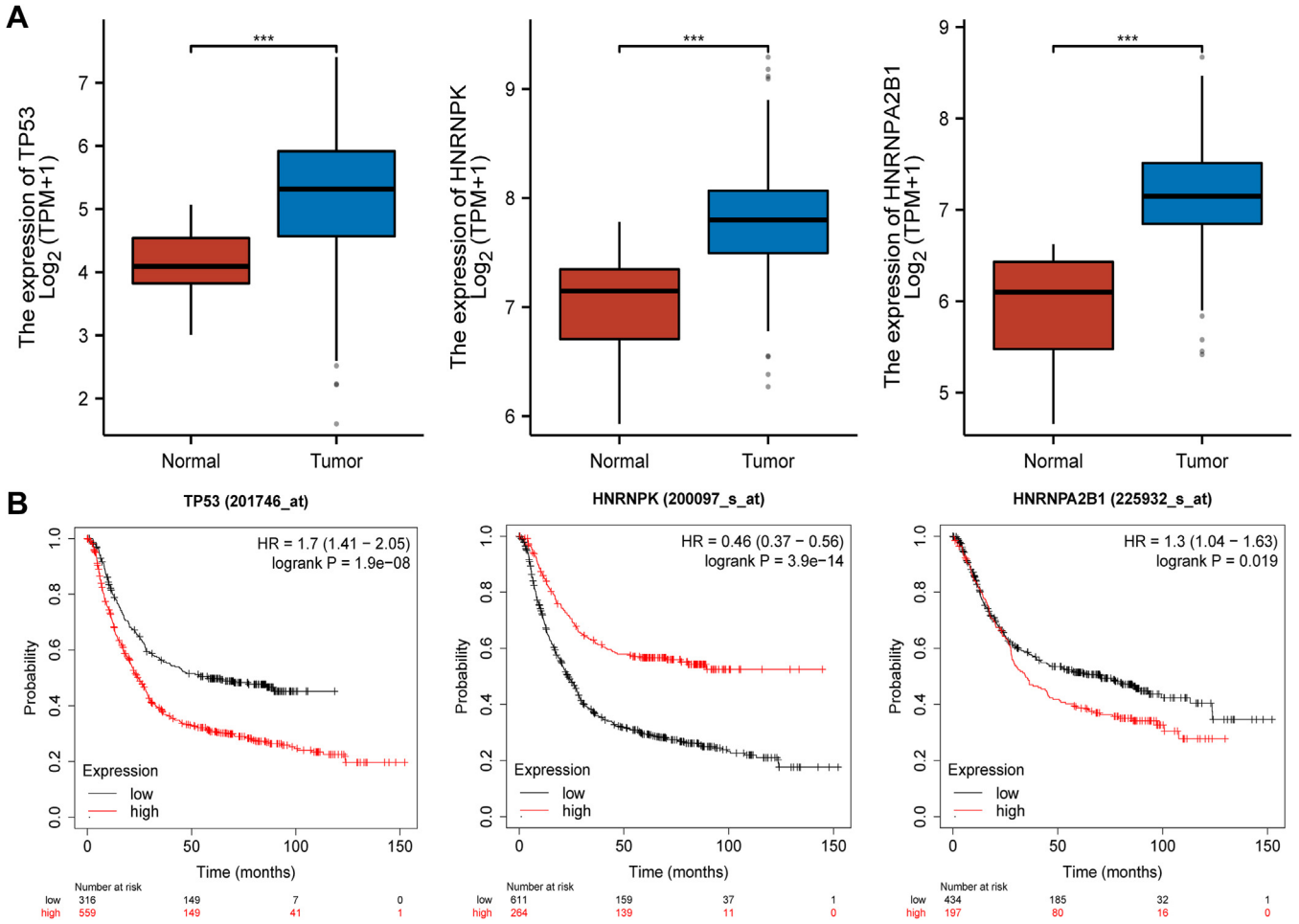

Figure 2. Expression and prognostic relevance of differentially expressed hnRNPs genes in GC. *A*, analysis of the expression of three candidate target genes in 32 normal gastric tissues and 375 GC gastric tissues. *B*, investigation of the relationship between the expression of three candidate target genes and the survival rate of GC patients.

mitochondrial metabolic reprogramming. Taken together, HNRNPA2B1 may play a role in GC tissues by regulating mitochondrial metabolic reprogramming.

In summary, HNRNPA2B1 may play a role in GC tissue by regulating mitochondrial metabolic reprogramming.

Enhanced expression of HNRNPA2B1 gene in GC tissues

To evaluate the protein expression level of the HNRNPA2B1 gene, we utilized the HPA database, IHC. The results revealed differential expression levels of HNRNPA2B1 in normal and GC tissue. Specifically, in normal tissue, HNRNPA2B1 exhibited moderate cytoplasmic staining, while in GC tissue, it exhibited intense cytoplasmic staining (Fig. 5).

High expression of HNRNPA2B1 in the GC microenvironment and its association with cell composition

We successfully downloaded the GC-related single-cell RNA sequencing dataset GSE163558 from the GEO database and conducted data quality control and gene expression matrix generation using Cell Ranger software. After filtering, we obtained high-quality cell samples. Furthermore, we performed clustering analysis using the Seurat package, resulting in the identification of up to 24 distinct cell clusters (Fig. 6*A*). The cell counts for each cluster varied from a few tens to several hundreds, highlighting the diversity of the tumor microenvironment. Subsequently, based on known marker genes, we annotated different cell types, using LUM for fibroblasts, CD3D for T cells, LGR5 for GCSCs, CD68 for macrophages, MS4A1 for B cells, S100A8 for neutrophils, RGS5 for dendritic cells, CDH5 for endothelial cells, MZB1 for plasma cells, S100 B for Schwann cells, PRSS1 for acinar cells, FGFBP2 for NK cells, and CHGA for endocrine cells, respectively (Fig. 6*B*). Moreover, we compared the abundance ratios of different cell clusters between normal and cancerous gastric gland tissues and found a substantial increase in the content of macrophages, GCSCs, and neutrophils in GC tissues compared to normal tissues (Fig. 6, *C* and *D*). Additionally, we utilized the FindAllMarkers function to analyze the expression pattern of HNRNPA2B1 in different cell types between normal and GC tissues. Our analysis revealed a significant upregulation of HNRNPA2B1 in macrophages, GCSCs, and neutrophils in GC tissues compared to normal tissues (Fig. 6*E*). HNRNPA2B1 is a nuclear ribonucleoprotein that plays a role in various BP, including gene expression regulation, mRNA processing, and stability (25). It maintains the malignant phenotype of GC by

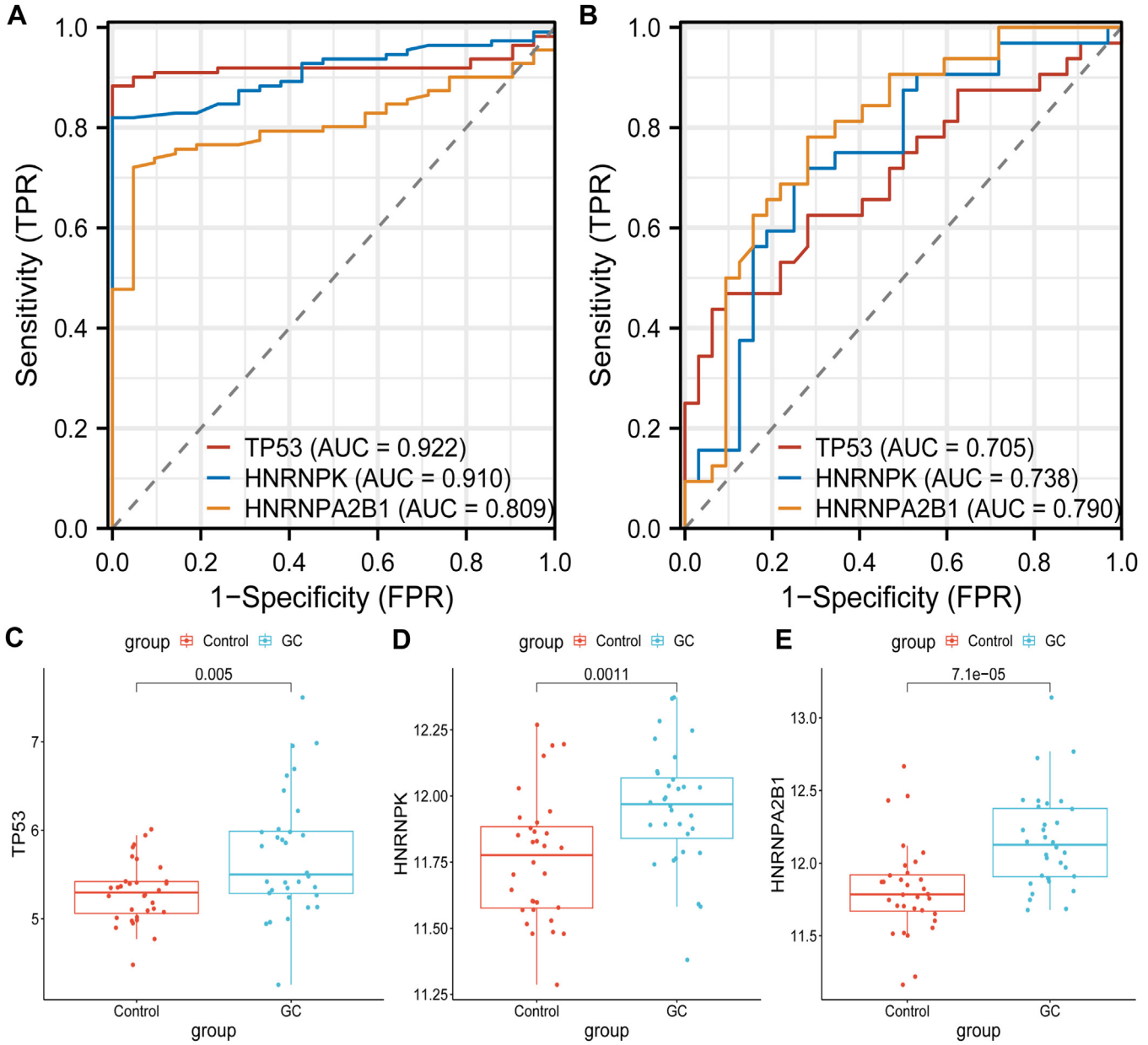

Figure 3. Further screening of target genes using ROC analysis. *A*, the diagnostic performance of candidate target genes in the training set of the GSE54129 dataset, represented by the AUC. The AUC value is used to measure the accuracy of the prediction, with an AUC value of one indicating perfect prediction, >0.90 indicating high accuracy, 0.70 to 0.90 indicating moderate accuracy, and 0.50 to 0.70 indicating low accuracy. *B*, the diagnostic performance of candidate target genes in the validation set of the GSE65801 dataset. *C–E*, box plots showing the expression levels of different genes in the control group and GC patients in the validation set of the GSE65801 dataset (Control = 32, GC = 32). If the *p*-value is less than 0.05, it is considered to have a significant difference.

promoting cell proliferation, inhibiting apoptosis, and facilitating cell migration. Studies have shown that GCSCs are the source of tumor recurrence and metastasis, as well as the cause of chemoresistance.

Therefore, the high expression of HNRNPA2B1 in GCSCs may contribute to increased cancer cell migration and the worsening condition of GC patients.

Deletion of HNRNPA2B1 increases the sensitivity of GCSCs to drugs

To verify the effects of HNRNPA2B1 knockout on GCSCs, we obtained highly purified $CD24^+$ $CD44^+$ GCSCs through flow cytometry. After long-term culture, flow cytometry was used to detect the expression of surface markers CD54 and EpCAM (Fig. S1*A*). Additionally, a CCK8 assay was performed to investigate the growth rate of the $CD24^+$ $CD44^+$ cell subpopulation (GCSCs) in MKN-45 cells after HNRNPA2B1 knockout. The results showed (Fig. S2, *A–C*) that compared to parental MKN-45 GCSCs, HNRNPA2B1 knockout affected GCSC proliferation, reducing the growth rate. The cells sorted in Figure 7*A* and Fig. S1*A* provided high-quality samples for subsequent experiments. Flow cytometry results indicated that, with increased culture time and cell passage, $CD24^+$ $CD44^+$ GCSCs exhibited a slight decrease in CD54 and

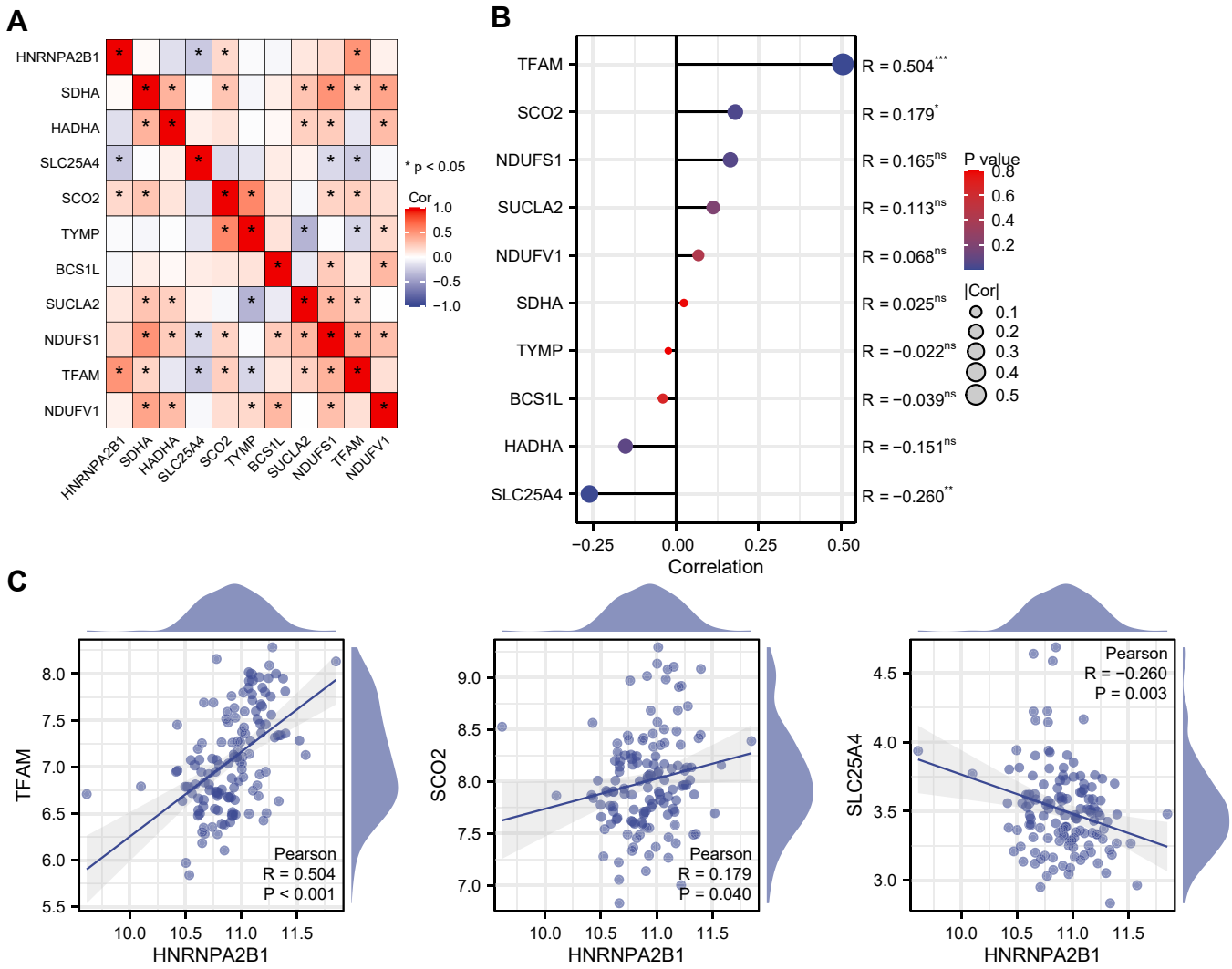

Figure 4. Correlation analysis of HNRNPA2B1 with mitochondrial metabolic reprogramming. *A* and *B*, heatmap (*A*) and lollipop plot (*B*) of Pearson correlation analysis between HNRNPA2B1 and the top 10 genes closely related to mitochondrial metabolic reprogramming. *C*, Scatter plots showing the correlation between HNRNPA2B1 and TFAM, SCO2, and SLC25A4.

EpCAM expression, but they still maintained stem cell properties.

We further assessed the expression levels of CD24, CD44, CD54, and EpCAM in both the parental GCSCs and HNRNPA2B1-knockout GCSCs. HNRNPA2B1 knockout significantly reduced their expression. Subsequently, immunofluorescence staining was performed on the $CD24^+$ $CD44^+$ and $CD24^-$ $CD44^-$ subpopulations to detect the expression of GC stem cell markers CD54 and EpCAM. The staining results showed that CD54 and EpCAM expression in the $CD44^+$ $CD24^+$ subpopulation was significantly higher than in the parental GCSCs and $CD44^-$ $CD24^-$ subpopulation (Figs. 7*B* and S1*B*). RT-PCR and Western Blot (WB) analysis confirmed that the expression of HNRNPA2B1 was significantly higher in the $CD24^+$ $CD44^+$ subpopulation compared to the parental cells and $CD44^-$ $CD24^-$ subpopulation (Figs. 7, *C* and *D*, and S1, *C* and *D*).

Next, we used CRISPR-Cas9 to knock out HNRNPA2B1 in MKN-45 and TMK-1 GCSCs, followed by gene rescue. We transfected HNRNPA2B1-knockout GCSCs with a plasmid overexpressing HNRNPA2B1 to determine its phenotypic effects. RT-PCR and WB results showed that, in the HNRNPA2B1-KO group, HNRNPA2B1 mRNA and protein levels were undetectable compared to the NC-KO group. Upon re-expression of HNRNPA2B1, both mRNA and protein levels were restored (Figs. 7, *E* and *F*, and S1*E*).

Finally, we evaluated the sensitivity of wild-type and HNRNPA2B1-knockout GCSCs to commonly used chemotherapeutic drugs. The results showed that the HNRNPA2B1-KO group had significantly enhanced drug sensitivity compared to the NC-KO group while restoring HNRNPA2B1 reduced this sensitivity (Fig. 7*G*). These results suggest that the loss of HNRNPA2B1 increases the sensitivity of GCSCs to chemotherapy drugs.

HNRNPA2B1 knockout suppresses migration, invasion, and proliferation of GCSCs from GC cell lines and induces apoptosis

To further investigate the effects of HNRNPA2B1 knockout on the function of MKN-45-derived GCSCs, we first performed

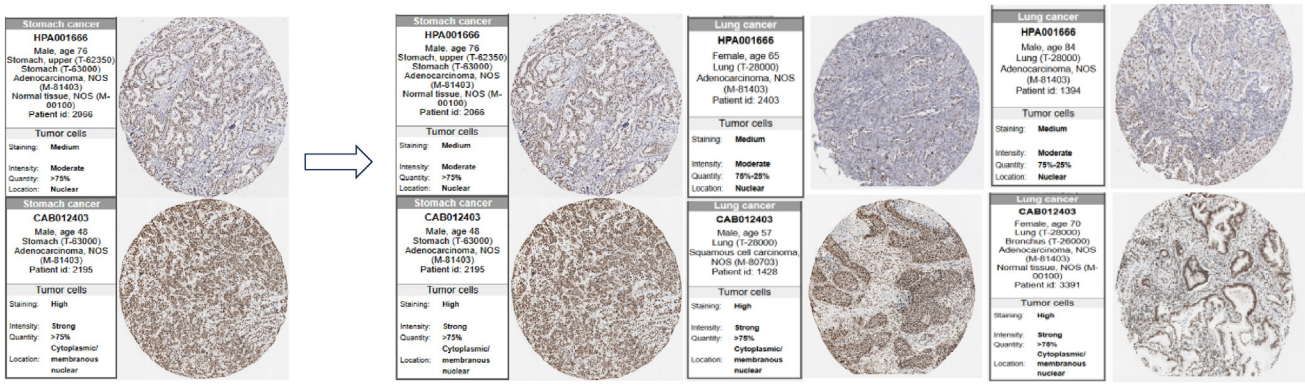

Figure 5. Immunohistochemical analysis of HNRNPA2B1 protein.

a scratch assay to assess changes in the migration ability of MKN-45-derived GCSCs. The results showed that compared to the NC-KO group, the migration ability of MKN-45-derived GCSCs in the HNRNPA2B1-KO group was significantly reduced (Fig. 8*A*). Transwell assays further revealed that the invasion ability of MKN-45-derived GCSCs in the HNRNPA2B1-KO group was also significantly decreased (Fig. 8*B*). Sphere formation assays confirmed that the sphere formation efficiency of MKN-45-derived GCSCs in the HNRNPA2B1-KO group was significantly reduced (Fig. 8*C*).

TUNEL assays were used to evaluate apoptosis in MKN-45-derived GCSCs. Cells were first treated with Genipin (HY-17389, MCE), then fixed with 4% paraformaldehyde, and permeabilized with 0.5% Triton-X 100. An *in situ* cell death detection kit (Roche, Basel, Switzerland) was used to stain the cells. The results showed that after treatment with 5-FU, the apoptosis rate in the NC-KO group was about 20%. In contrast, the apoptosis rate was significantly higher in the HNRNPA2B1-KO group (Fig. 8*D*).

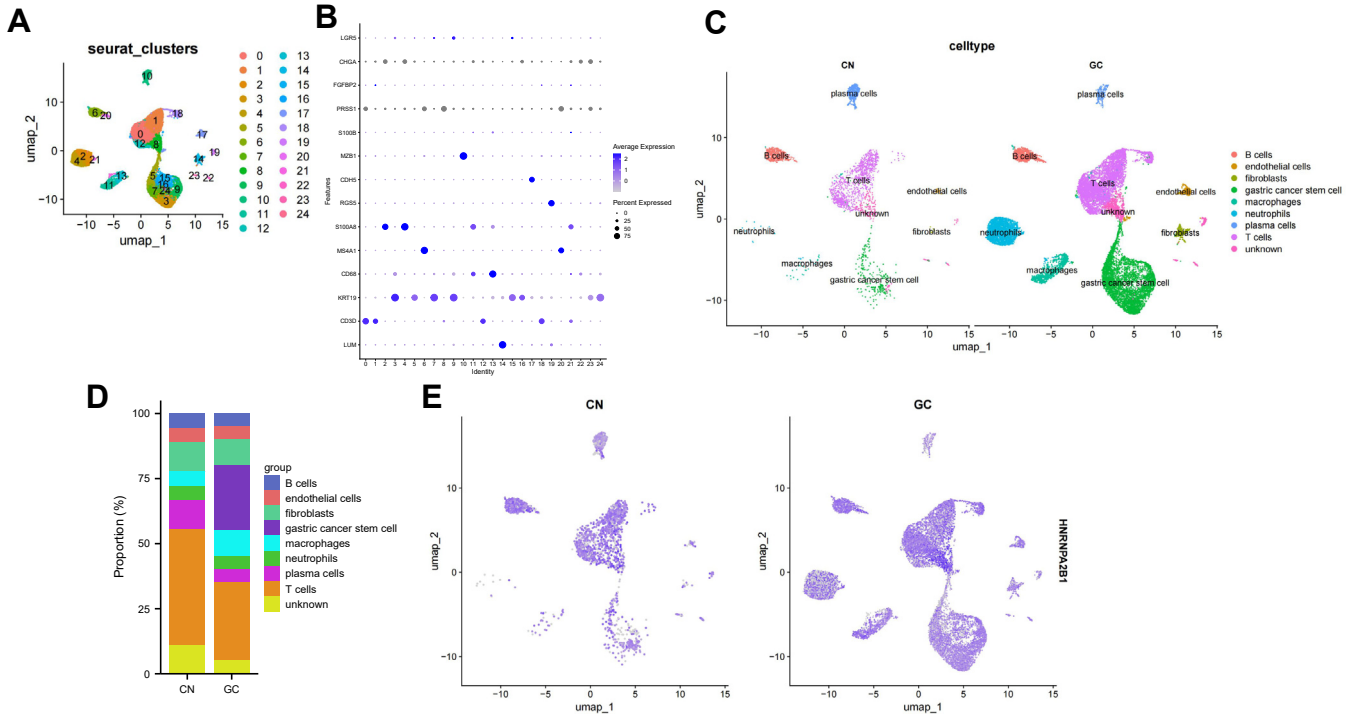

Figure 6. Single-cell analysis of the HNRNPA2B1 gene. *A*, The cell clustering results were obtained using a resolution parameter of 1.0. *B*, different cell populations using marker genes such as LUM and CD3D. *C*, the compositional differences between GC cells and normal pancreatic cells. *D*, cell proportions in different samples. *E*, the expression of the HNRNPA2B1 gene in different cells from normal and GC tissues.

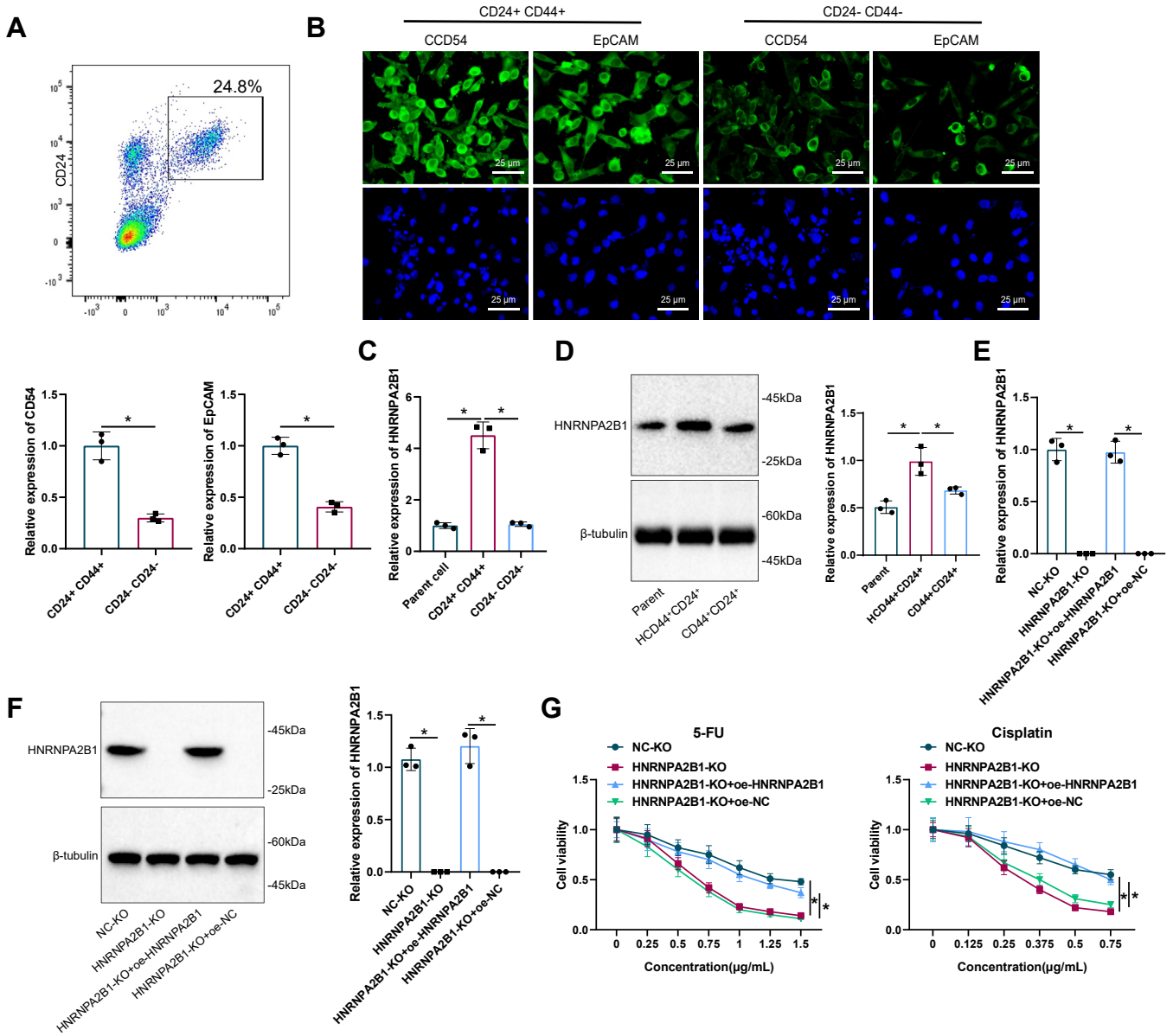

Figure 7. Knockdown of the key factor HNRNPA2B1 enhances drug sensitivity in GCSCs. *A*, $CD24^+$ $CD44^+$ GCSC were sorted from MKN-45 cells using flow cytometry. *B*, immunofluorescence staining was employed to detect the expression of the stem cell markers CD54 and EpCAM in $CD24^+$ $CD44^+$ GCSC. *C*, RT-PCR was used to measure the expression level of HNRNPA2B1 mRNA in GCSC cells. *D*, WB was conducted to examine the expression of HNRNPA2B1 protein in GCSC cells. *E*, RT-PCR was performed to assess the expression level of HNRNPA2B1 mRNA in GCSC cells after CRISPR-Cas9 knockout. *F*, WB was utilized to analyze the expression of HNRNPA2B1 protein in GCSC cells after CRISPR-Cas9 knockout. *G*, CCK8 assay was utilized to evaluate the sensitivity of GCSC cells with HNRNPA2B1 knockout to commonly used chemotherapeutic drugs. * indicates $p < 0.05$, and all cell experiments were performed with three biological replicates.

Additionally, WB results indicated that compared to the NC-KO group, the expression of the proliferation marker protein Ki67 and the migration/invasion marker protein Vimentin was significantly reduced in the HNRNPA2B1-KO group. E-cadherin expression was significantly increased, while the apoptosis marker protein Bax was upregulated and Bcl-2 was downregulated. The cleavage of the caspase substrate PARP-1 and the amount of cleaved caspase-3 were also significantly elevated (Fig. 8*E*).

When we restored HNRNPA2B1 expression, the inhibitory effects on migration, invasion, and proliferation in MKN-45-derived and TMK-1-derived GCSCs were reversed, and apoptosis was suppressed. The protein expression trends in TMK-1-derived GCSCs were consistent with those in MKN-45-derived GCSCs (Fig. S3).

These results suggest that HNRNPA2B1 plays an indispensable role in maintaining the stemness of MKN-45-derived and TMK-1-derived GCSCs and inhibiting apoptosis in GCSCs.

HNRNPA2B1 depletion suppresses mitochondrial function and structure in GCSCs

Bioinformatics analysis previously revealed that HNRNPA2B1 is associated with mitochondrial metabolism.

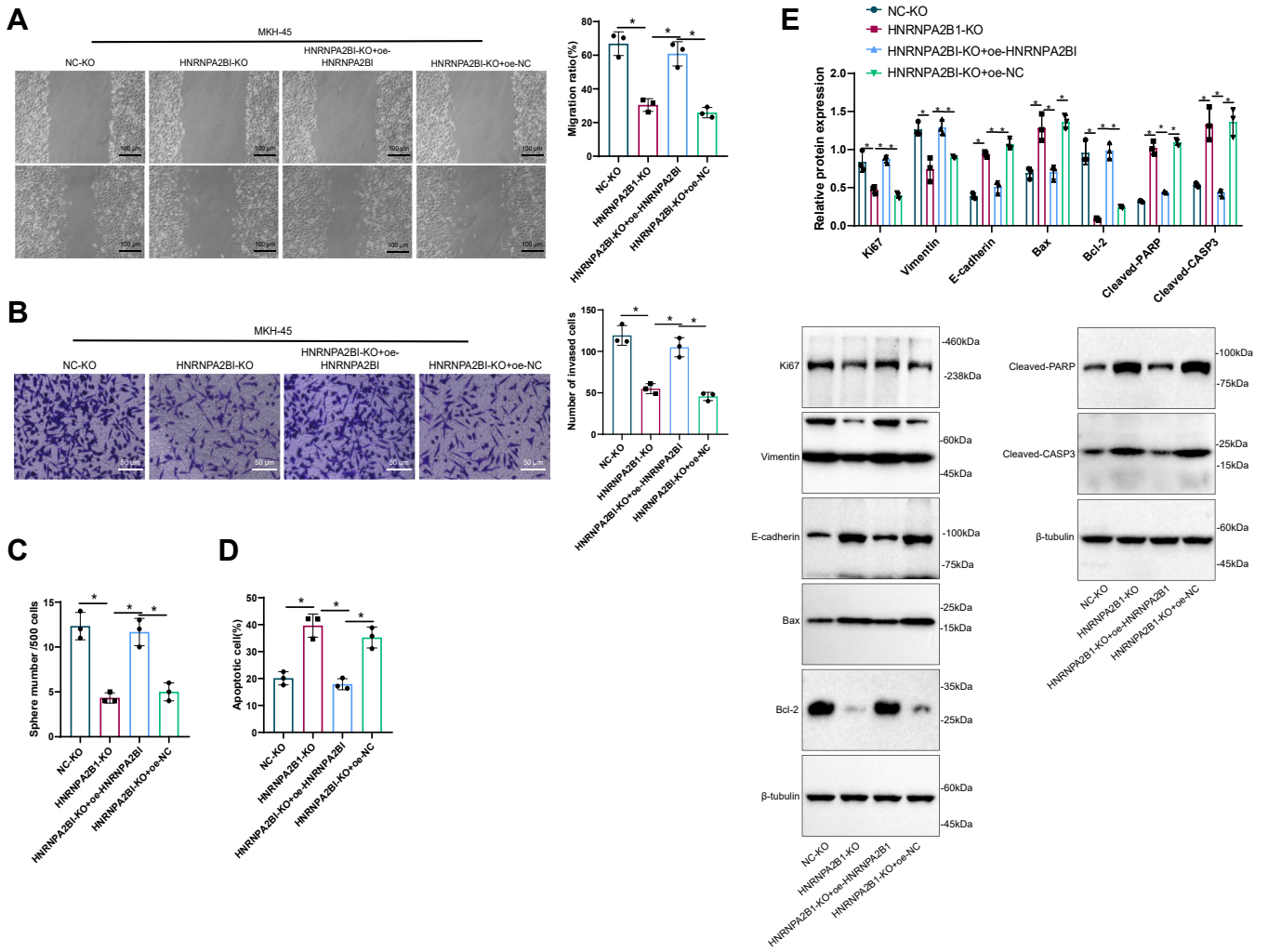

Figure 8. Knockdown of HNRNPA2B1 affects migration, invasion, sphere formation, and apoptosis of GCSCs. *A*, scratch experiment was conducted to examine the changes in migration ability of GCSC cells after HNRNPA2B1 knockout. *B*, transwell assay was employed to assess the invasion ability of GCSC cells after HNRNPA2B1 knockout. *C*, sphere formation experiments were performed to evaluate the sphere-forming ability of GCSC cells after HNRNPA2B1 knockout. *D*, TUNEL assay was used to detect the apoptosis of GCSC cells after HNRNPA2B1 knockout. *E*, WB was carried out to analyze the expression of proliferation, migration, invasion, and apoptosis marker proteins in GCSC cells after HNRNPA2B1 knockout. * indicates $p < 0.05$, and all cell experiments were performed with three biological replicates.

To verify whether HNRNPA2B1 similarly regulates mitochondrial energy metabolism in GCSCs, we first measured the resting oxygen consumption rate (OCR) in different MKN-45-derived GCSCs. The results showed that compared to the NC-KO group, the OCR in MKN-45-derived GCSCs from the HNRNPA2B1-KO group was significantly reduced (Fig. 9*A*), indicating a decrease in mitochondrial oxidative phosphorylation efficiency. When HNRNPA2B1 was re-expressed, the OCR increased, suggesting that oxidative phosphorylation efficiency was restored. Additionally, the extracellular acidification rate (ECAR) measurement in different MKN-45-derived GCSCs revealed that, compared to the NC-KO group, ECAR was significantly elevated in the HNRNPA2B1-KO group (Fig. 9*B*), indicating activation of glycolysis. This effect was reversed upon re-expression of HNRNPA2B1.

Next, we assessed the changes in mitochondrial membrane potential in different MKN-45-derived GCSCs. The results showed that the red/green fluorescence ratio was significantly decreased in the HNRNPA2B1-KO group compared to the NC-KO group (Fig. 9*C*). After HNRNPA2B1 re-expression, the red/green fluorescence ratio increased in MKN-45-derived GCSCs. Similarly, ROS detection results indicated that ROS levels were significantly elevated in the HNRNPA2B1-KO group compared to the NC-KO group (Fig. 9*D*), and ROS levels were reduced when HNRNPA2B1 was re-expressed.

Mitochondrial morphology analysis revealed that, compared to the NC-KO group, MKN-45-derived GCSCs in the HNRNPA2B1-KO group exhibited fewer mitochondria, irregular sizes, and structural abnormalities, specifically characterized by a reduction in mitochondrial cristae and increased transparency of the mitochondrial matrix. These mitochondrial defects were notably restored upon HNRNPA2B1 re-expression (Fig. 9*E*).

In conclusion, these results further confirm that HNRNPA2B1 knockout inhibits mitochondrial function and structure in GCSCs.

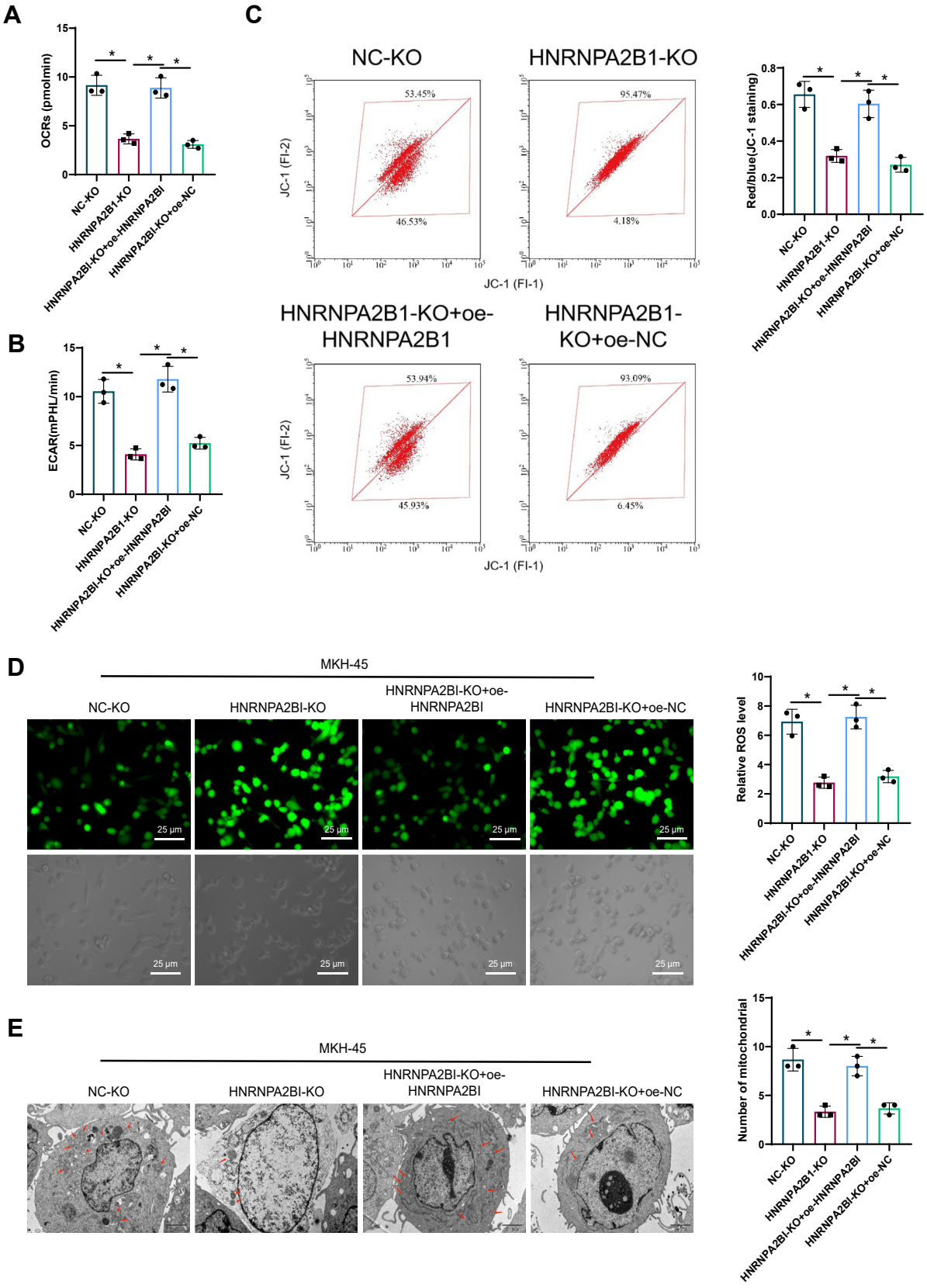

Figure 9. Knockdown of HNRNPA2B1 affects mitochondrial energy metabolism in GCSCs. *A*, measurement of the resting OCR in GCSC cells after HNRNPA2B1 knockout. *B*, detection of the ECAR in GCSC cells after HNRNPA2B1 knockout. *C*, assessment of changes in mitochondrial membrane potential in GCSC cells after HNRNPA2B1 knockout using flow cytometry and JC-1 staining. *D*, evaluation of changes in ROS levels in GCSC cells after HNRNPA2B1 knockout using DCFDA. *E*, observation of mitochondrial morphology changes in GCSC cells after HNRNPA2B1 knockout using TEM (*red* arrows indicate mitochondria, bar value indicates one um). * indicates $p < 0.05$, and all cell experiments were performed with three biological replicates.

HNRNPA2B1 induces chemoresistance in GCSCs by inhibiting apoptosis and promoting proliferation In vivo

First, MKN-45-derived GCSC cells were treated with 5-Fu to establish a chemoresistant MKN-45-derived GCSC cell line. This resistant cell line was then used to establish a subcutaneous xenograft model in athymic nude mice to explore the effects of HNRNPA2B1 knockout on the tumorigenicity of MKN-45-derived GCSCs *in vivo* and to investigate whether HNRNPA2B1 contributes to GCSC chemoresistance *in vivo*. Resistant NC-KO or HNRNPA2B1-KO TMK-1-derived GCSCs were subcutaneously implanted into athymic nude mice, followed by 5-Fu treatment. The results showed that, compared to the NC-KO group treated with 5-Fu, the tumor volume and weight were significantly reduced in the HNRNPA2B1-KO group treated with 5-Fu (Fig. S4*A*).

The Ki-67 proliferation index is commonly used to assess tumor proliferation, and cleaved Caspase-3 serves as an early marker of apoptosis. Therefore, immunohistochemistry (IHC) staining with anti-Ki-67 and anti-cleaved Caspase-3 antibodies was performed on serial sections of xenograft tumor samples to investigate the role of HNRNPA2B1 in cell proliferation and apoptosis *in vivo*. IHC staining showed fewer Ki-67-positive cells and more cleaved Caspase-3-positive cells in the HNRNPA2B1-KO+5-Fu group compared to the NC-KO+5-Fu treatment group (Fig. S4*B*).

In addition, flow cytometry was used to assess the proportion of $CD24^+$ $CD44^+$ positive subpopulations within tumors in both groups of mice. The results revealed that the HNRNPA2B1-KO+5-Fu group had a significantly lower percentage of $CD24^+$ $CD44^+$ cells compared to the NC-KO+5-Fu treatment group, indicating that HNRNPA2B1 knockout inhibited tumor stemness (Fig. S4*C*). These *in vivo* observations confirm that HNRNPA2B1 promotes GCSC chemoresistance by inhibiting apoptosis and promoting proliferation, and that knockout of this gene significantly reduces the tumorigenicity and chemoresistance of GCSCs *in vivo*.

Discussion

GCSCs play a crucial role in the occurrence, development, and recurrence of GC, as they represent a small subset of cells with self-renewal and multi-directional differentiation potential (31, 32). These cells possess robust proliferative and anti-apoptotic abilities, which contribute to the increased difficulty in treatment (33, 34). Previous studies have suggested a close association between the existence of GCSCs and malignant behaviors such as chemoresistance, tumor recurrence, and metastasis (31, 32). Consequently, investigating the biological characteristics and regulatory mechanisms of GCSCs holds significant importance in improving the effectiveness of GC treatments (Fig. 10).

In other types of tumors, studies have shown that heterogeneous nuclear ribonucleoprotein HNRNPA2B1 plays an important role in cell proliferation, apoptosis, and metastasis (9, 35, 36). In comparison to previous research, this study is the first to explore the function of HNRNPA2B1 in GCSCs (9, 35, 36). Through systematic analysis of GC datasets, this study identified HNRNPA2B1 as a key candidate gene, and experiments such as immunofluorescence confirmed its significant upregulation in MKN-45-derived GCSCs.

Using CRISPR-Cas9 technology, this study successfully knocked out the HNRNPA2B1 gene. Further cellular experiments demonstrated that HNRNPA2B1 knockout enhanced the sensitivity of MKN-45-derived and TMK-1-derived GCSCs to chemotherapeutic drugs, including 5-FU and cisplatin, suggesting that HNRNPA2B1 is a critical factor in regulating chemoresistance in GCSCs.

Further results showed that HNRNPA2B1 knockout inhibited the migration, invasion, and sphere-forming abilities of MKN-45-derived and TMK-1-derived GCSCs. Additionally, HNRNPA2B1 knockout increased the apoptosis rates of MKN-45-derived and TMK-1-derived GCSCs, further proving the key role of HNRNPA2B1 in GCSCs.

This study also found that HNRNPA2B1 knockout led to alterations in the metabolic reprogramming process of GCSCs. HNRNPA2B1 knockout reduced the number of mitochondria, resulting in instability in mitochondrial size and abnormal structure within the cells. Furthermore, HNRNPA2B1 knockout decreased the resting OCR, increased the ECAR, lowered mitochondrial membrane potential, and elevated ROS levels.

In summary, this study comprehensively analyzed RNA sequencing and proteomic data from the GC dataset and identified hnRNP HNRNPA2B1 as a key player in GCSCs. Our findings indicate that the expression of HNRNPA2B1 is closely correlated with the progression and prognosis of GC. The selection of DEGs revealed multiple important metabolic pathways associated with GC development, such as RNA transport, cell cycle, and cancer pathways. Further experiments confirming the knockout of HNRNPA2B1 demonstrated its significant role in maintaining the stemness, metabolic state, and drug sensitivity of GCSCs. Specifically, HNRNPA2B1 knockout resulted in significant changes in mitochondrial energy metabolism in GCSCs, characterized by decreased oxidative phosphorylation efficiency and activated glycolysis.

The scientific value of this study lies in revealing the mechanistic role of hnRNP HNRNPA2B1 in GCSCs, particularly in the metabolic reprogramming and chemoresistance formation of these cells. Through gene knockout experiments and functional assays on GCSCs, researchers found that the upregulation of HNRNPA2B1 enhanced resistance to chemotherapy drugs and increased cell migration, invasion, and anti-apoptotic abilities. Additionally, HNRNPA2B1 further promoted chemoresistance and cancer progression in GCSCs by inducing mitochondrial dysfunction and metabolic reprogramming. These findings highlight the potential therapeutic application of HNRNPA2B1 in GC treatment and provide a theoretical basis for the development of new treatment strategies.

However, this study has some limitations. The research primarily focused on the impact of HNRNPA2B1 and its relationship with GCSCs, but further investigation is needed to explore the expression and function of HNRNPA2B1 in other

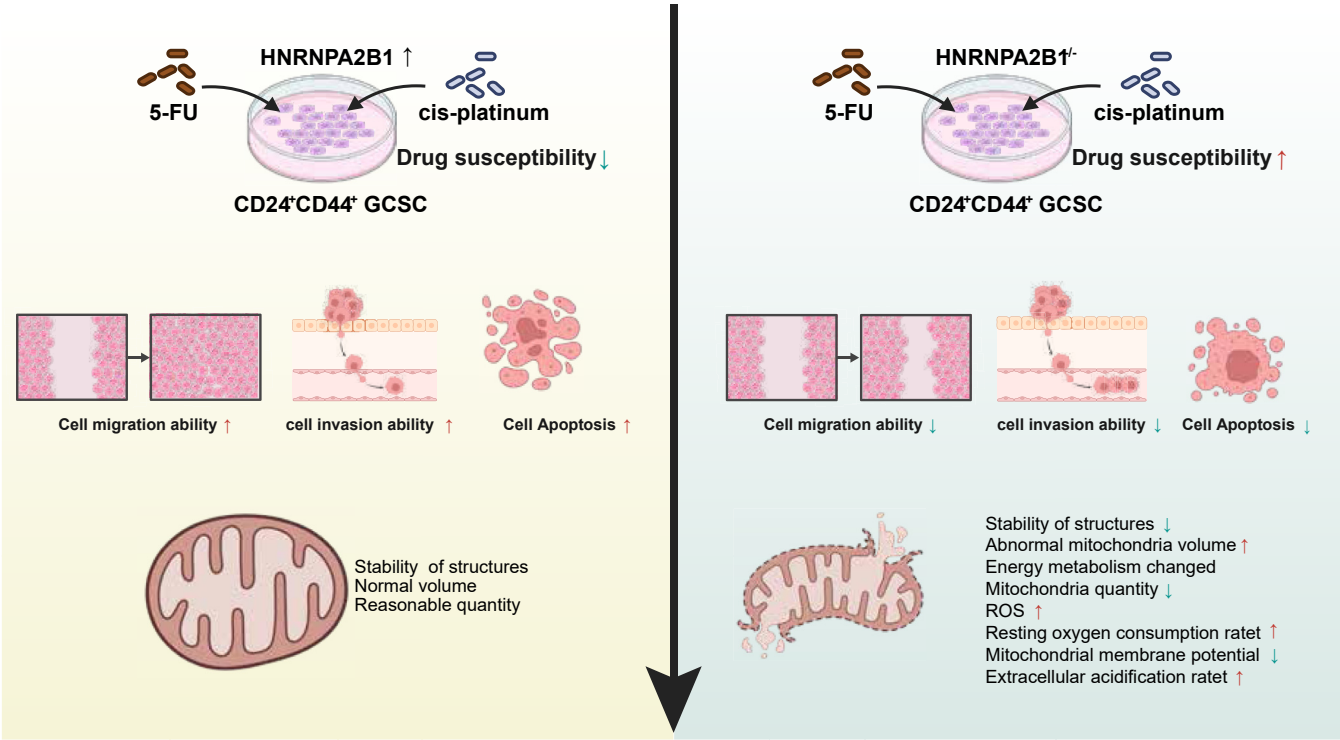

Figure 10. Mechanism of action of HNRNPA2B1 in GCSCs. HNRNPA2B1 regulates mitochondrial metabolism to sustain the malignant phenotype of GCSCs, enhancing their migration, invasion, and drug resistance. Knocking out HNRNPA2B1 disrupts these processes and increases drug sensitivity.

GC cell types and different tumor types. Additionally, although gene knockout validation was performed using CRISPR-Cas9 technology, further studies are required to determine whether other factors may interfere with or affect the function of HNRNPA2B1.

Looking ahead, studies have shown that HNRNPA2B1 can interact directly with the transcriptional coactivator p300. Acetylation of HNRNPA2B1 by p300 promotes its binding to the cyclooxygenase-2 (COX-2) promoter, thereby increasing COX-2 expression and enhancing the proliferative capacity of non-small cell lung cancer cells (37). Other reports suggest that the metastasis suppressor gene Nm23-H1 can increase the stability of the HNRNPA2B1 protein, allowing it to be co-recruited to the 5′UTR of specific protein-1 (Sp1) mRNA, enhancing Sp1 translation activity. Sp1 is upregulated in early lung cancer and downregulated at later stages. These findings indicate that HNRNPA2B1 may not only serve as a biomarker for the early diagnosis of lung cancer but also as a prognostic indicator and a potential therapeutic target for lung cancer (38). The main limitations include the lack of specific ligands for HNRNPA2B1, unclear mechanisms of tumor suppression, and the untapped potential of chemically targeting HNRNPA2B1 for anticancer therapy. Therefore, further validation of HNRNPA2B1's potential therapeutic applications in GC holds great promise. Future research can delve deeper into the regulatory mechanisms of HNRNPA2B1, such as its miRNA regulatory network, to further reveal its mechanism of action in GCSCs. By thoroughly studying the function of HNRNPA2B1, researchers may provide theoretical support for discovering new targeted treatment strategies and drugs, improving treatment outcomes for GC patients, and reducing the risks of treatment resistance and recurrence.

Experimental procedures

Dataset acquisition and filtering

The GC expression profile dataset GSE54129 was retrieved from the GEO database (https://www.ncbi.nlm.nih.gov/gds). This dataset includes 111 GC tissues and 21 non-GC tissues, which were used as the training set. The sequencing platform used was GPL570 (39). Additionally, the GC expression profile dataset GSE65801 was downloaded as the validation set. This dataset consists of 32 GC tissues and 32 non-GC tissues, with the sequencing platform being GPL14550. To validate the expression levels, data from the public database TCGA was accessed, including a total of 407 samples, which comprised 32 non-GC tissues and 375 GC tissues (40). Filtering criteria, including $|\log FC| > 0$ and a false discovery rate < 0.05, were applied to select DEGs using the R package "limma". The intersection of DEGs between the DEGs of the GSE54129 dataset and the GSE65801 dataset was identified for further analysis. All analyses were conducted using R version 4.3.1 (R Foundation for Statistical Computing) (41).

KEGG/GO functional enrichment analysis

To assess the functional relevance of DEGs in GC, GO, and KEGG pathway enrichment analyses were performed using the cluster Profiler package in R software. The GO enrichment analysis included BP, MF, and CC. The results were ranked based on their *p*-values and online tools were used for the

enrichment analysis of candidate targets. Additionally, the data was visualized using the ggplot2 package (42). A significance threshold for enrichment was set at a p-value less than 0.05.

Candidate target selection

The GC-related target genes and genes associated with hnRNPs were obtained from the GeneCards database (https://www.genecards.org/). A search using the terms "Gastric cancer" and "heterogeneous nuclear ribonucleoproteins" was conducted to retrieve a list of relevant genes. A filter of relevance score ≥ 10 was then applied to select GC-related target genes. The top 10 genes related to hnRNPs were chosen to ensure higher relevance for further analysis. Finally, the GC-related target genes, hnRNPs-related genes, and DEGs from the GEO chip analysis were combined through Venn analysis to obtain the candidate targets (42, 43).

Expression analysis and survival curve identification

Survival curves of candidate target genes in GC patients were constructed using the Kaplan-Meier Plotter database (kmplot.com). Gender and previous treatments were not considered. To plot the Kaplan-Meier graph, input the gene name and click "Plot Kaplan-Meier." The expression levels of the candidate genes in the control group and GC group were verified, and the non-parametric Wilcoxon test was used to compare the p-values between the two groups. The ggplot2 package in R was utilized to generate a boxplot, visually depicting the expression levels of the candidate target genes in the control and GC groups. A p-value less than 0.05 indicated a significant difference.

ROC curve for determining candidate genes

Using the pROC package in R, receiver operating characteristic (ROC) curves were plotted based on the expression values of the candidate genes, assessing the accuracy of predicting disease status within the training and validation datasets.

Pearson correlation analysis

The GeneCards database (https://www.genecards.org/) was employed to retrieve genes related to mitochondrial metabolic reprogramming. The keyword "Mitochondrial metabolic reprogramming" was used for the search, and a list of relevant genes was obtained. The top 10 genes exhibiting the strongest correlation with HNRNPA2B1 were selected, and their correlation was calculated using Pearson's statistics.

Protein expression verification of candidate genes

The Human Protein Atlas (HPA) protein database (https://www.proteinatlas.org/) utilizes transcriptomics and proteomics techniques to study RNA and protein levels in different tissues and organs of the human body, providing valuable information on protein expression. To date, the HPA database has collected over 26,000 antibodies. The protein expression information is derived from IHC staining, which is confirmed by professionals, ensuring high accuracy and reliability. Therefore, we utilized the HPA database to validate the protein levels of iron death-related genes (44).

Acquisition and preprocessing of single-cell RNA sequencing data

The GC-related single-cell RNA sequencing dataset GSE163558 was downloaded from the GEO database (https://www.ncbi.nlm.nih.gov/geo/), which includes 3 GC samples (GSM5004180, GSM5004181, and GSM5004182) and one adjacent carcinoma sample (GSM5004183). The raw sequence files were quality-controlled, and gene expression matrices were generated using Cell Ranger software (version 3.0.2, 10x Genomics). The raw single-cell RNA sequencing data was further quality-controlled and normalized using the Seurat package (version 3.2.1). Cells with low gene expression and abnormal gene counts were filtered out to ensure data quality and consistency. Principal component analysis (PCA) was performed using Seurat to reduce the dimensionality of the data and highlight major variations between cells. The main principal components were selected for subsequent clustering and visualization analysis. Cell clusters were identified using graph-based clustering methods. The resolution parameter was adjusted to determine the optimal number of cell clusters, ensuring biologically meaningful clustering results. For each cell cluster, known cell type marker genes were annotated to identify different cell types and states, and reference to publicly available cell type annotation databases was made to enhance the accuracy and completeness of the annotations.

Procurement and cultivation of GC cells

The GC cell line used in this study was MKN-45 (CL-0292, Pronosai) and TMK-1 (XY-H790, Shanghai Xinyu Biotechnology Co., Ltd). These cells were cultured in RPMI 1640 medium (11875168, Gibco) containing 10% fetal bovine serum (12484028, Gibco) and 1% penicillin-streptomycin (15140148, Gibco). The cells were maintained at 37 °C in a CO_2 incubator (model NX7LIVE001, Thermo Fisher Scientific, USA) (45).

Flow cytometry for $CD24^+$ $CD44^+$ positive cell screening

First, MKN-45 or TMK-1 cells were counted and transferred to 5 ml centrifuge tubes. The cells were washed twice with HBSS containing 2% FBS (H6648, Sigma). Next, anti-CD44-PE (ab269300, Abcam) and anti-CD24-FITC (ab30350, Abcam) antibodies were added, and the samples were incubated on ice for 20 min. After incubation, the cells were washed again and resuspended in HBSS/2% FBS containing 4′,6-diamidino-2-phenylindole (DAPI; D9542, Merck) at a final concentration of 1 μg/ml. Flow cytometry (BD Biosciences, USA) was then used to sort $CD24^+$ $CD44^+$ positive GCSCs, where MKN-45-derived GCSCs and TMK-1-derived GCSCs were obtained. The sorted cells were cultured in tumor stem cell sphere medium (P2401, Shanghai Qida Biotechnology), and passage three cells were used for subsequent experiments (46).

Immunofluorescence staining

Immunofluorescence staining was performed on the sorted $CD24^+$ $CD44^+$ and $CD24^-$ $CD44^-$ subpopulations to detect the expression of GC stem cell markers CD54 and EpCAM, confirming their stemness ($CD54^+$ $EpCAM^+$). The stability of the $CD24^+$ $CD44^+$ subpopulation during long-term culture was assessed by periodically analyzing surface marker expression (CD54 and EpCAM) using flow cytometry after 3 to 5 passages. Stable marker expression indicated that the cells maintained their stemness. After HNRNPA2B1 knockout in MKN-45-derived GCSCs using CRISPR-Cas9, immunofluorescence staining for CD24, CD44, CD54, and EpCAM was performed. The cells were incubated with Alexa Fluor 647-labeled anti-CD44 antibody (ab314280, Abcam), anti-CD24 antibody (ab237291, Abcam), Alexa Fluor 488-labeled anti-CD54 antibody (ab214860, Abcam), and EpCAM antibody (ab313667, Abcam) at recommended concentrations. Imaging was carried out using a fluorescence microscope (Olympus Corporation, Japan) (47).

Establishment of 5-FU resistant MKN-45-derived GCSCs

To establish a 5-FU-resistant cell line from MKN-45-derived GCSCs, we used repeated high-dose shocks combined with gradual drug concentration increases. Logarithmic-phase MKN-45-derived GCSCs were incubated in 10 mg/L 5-FU for 24 h at 37 °C in a 5% CO_2 incubator. After washing with Ca^{2+}-free and P_3-free phosphate-buffered saline, the cells were cultured in drug-free RPMI 1640 medium until they recovered. This process was repeated seven times over 4.5 months, resulting in the establishment of the resistant cell line MKN-45/5-FU. The cells were then maintained in RPMI 1640 medium containing 40 mg/L 5-FU, with passaging every 2 to 3 days for subsequent experiments (48).

CRISPR-Cas9 knockout of HNRNPA2B1 in MKN-45-derived GCSCs

The HNRNPA2B1 gene was targeted for knockout in GCSCs utilizing the CRISPR-Cas9 technique. Specifically designed sgRNA (sequence information in Table 1) was transfected into GCSCs along with the Cas9 protein complex. Transfection was performed using Lipofectamine CRISPRMAX Cas9 Transfection Reagent (CMAX00008, Invitrogen). Editing efficiency was verified through RT-qPCR, WB, and Sanger sequencing (49).

Gene rescue experiment

A lentiviral vector for overexpression of HNRNPA2B1 was constructed, with a strong promoter (such as the CMV promoter) used to drive the expression of the HNRNPA2B1 gene. Cells from HNRNPA2B1-knockout MKN-45-derived GCSCs and TMK-1-derived GCSCs were seeded and incubated overnight at 37 °C. Cells were then incubated with the overexpression plasmid and Lipofectamine 2000 (11,668–027, Invitrogen, CA, USA) in OPTI-MEM reduced-serum medium (Life Technologies) for 6 h. After incubation, the cells were washed, and a fresh medium was added to ensure stable plasmid expression. The experimental groups for MKN-45-derived GCSCs were KO-NC, HNRNPA2B1-KO, HNRNPA2B1-KO + oe-HNRNPA2B1, and HNRNPA2B1-KO + oe-NC. The same groupings were used for TMK-1-derived GCSCs. After plasmid transfection, phenotypic analyses, including cell proliferation, apoptosis, and migration assays, were conducted to assess the effects of HNRNPA2B1 restoration (50).

RT-qPCR

Total RNA was extracted from cultured cells using TRIzol reagent (15596018CN, Invitrogen) as per the manufacturer's instructions. 1 μg of total RNA was reverse-transcribed into cDNA using the reverse transcription system (Catalog Number 4366597, Invitrogen). qRT-PCR was performed using the SYBR GreenER qPCR SuperMix Universal kit (Catalog Number 11762500, Invitrogen). Relative gene expression was analyzed using the $2^{-\Delta\Delta Ct}$ method with GAPDH as the reference gene (51). Each experiment was repeated at least three times independently. Primer sequences and reference gene information can be found in Table 2.

WB

The M-PER mammalian protein extraction reagent (Thermo) was used to extract proteins from the cells. Total protein (30 μg) was quantified using the BCA protein determination assay kit (Thermo). The proteins were then separated by electrophoresis on a 10% or 6% sodium dodecyl sulfate-polyacrylamide gel. Subsequently, the proteins were transferred onto a 0.2 μm polyvinylidene fluoride (PVDF) membrane (ISEQ00010, Millipore). After the protein on the membrane was immobilized, blocking was performed using QuickBlock buffer (P0220, Beyotime Biotechnology). The membrane was incubated with the following antibodies overnight at 4 °C: rabbit anti-HNRNPA2B1 (1:1000, ab283592, Abcam), rabbit anti-Ki67 (1:1000, ab16667, Abcam), rabbit anti-Bcl-2 (1:2000, ab182858, Abcam), rabbit anti-Bax (1:5000, ab32503, Abcam), rabbit anti-E-Cadherin (1:10,000, ab40772, Abcam), rabbit anti-Vimentin (1:5000, ab92547, Abcam), rabbit anti-PARP1 (1:1000, ab137653, Abcam), rabbit anti-Caspase-3 (1:1000, ab32351, Abcam) and rabbit anti-β-

Table 1
CRISPR-Cas9 knockout HNRNPA2B1 sequence information

Name	Sequence (5′-3′)	PAM
sg-NC	AAAUGUGAGAUCAGAGUAAU	NA
sg-HNRNPA2B1	GAGGAACUACUACGAACAAU	GGG

Table 2
RT-qPCR primer sequence

Name	Sequence (5′-3′)
HNRNPA2B1	F: GGAGTGGAAGAGGAGGCAAC R: CAGGTCCTCCTCCATACCCA
GAPDH	F: GAGAAGGCTGGGGCTCATTT R: AGTGATGGCATGGACTGTGG

tubulin (1:500, ab6046, Abcam). The membrane was then washed three times with Tris-buffered saline containing 0.1% Tween 20 (TBST, Cat. No. ST671, Beyotime Biotechnology) and incubated with HRP-conjugated rabbit secondary antibody (1:10,000, ab6721, Abcam) at room temperature for 1 h. After three more washes with TBST, the proteins on the membrane were visualized using an enhanced chemiluminescence system. The grayscale values of the protein bands were analyzed using ImageJ software (51).

CCK-8 assay

The growth rate of GCSCs derived from parental and HNRNPA2B1 knockout MKN-45 cells was assessed using a CCK-8 assay. Specifically, parental and HNRNPA2B1 knockout MKN-45 cells were seeded into 96-well plates and cultured conventionally for 24, 48, 72, and 96 h. Subsequently, each well was treated with 10 μl of CCK-8 reagent (CA1210, Selleck) for 3 h at 37 °C. Absorbance at 450 nm was recorded using a microplate spectrophotometer (52).

To assess the sensitivity changes of GCSCs in both wild-type and HNRNPA2B1 knockout cells, they were treated with chemotherapeutic drugs. The drugs used were 5-fluorouracil (5-FU) (F6627, Sigma-Aldrich) at concentrations of 0 ug/ml, 0.25 ug/ml, 0.50 ug/ml, 0.75 ug/ml, 1.00 ug/ml, 1.25 ug/ml, and 1.5 ug/ml, and cisplatin (232,120, Sigma-Aldrich) at concentrations of 0 ug/ml, 0.125 ug/ml, 0.25 ug/ml, 0.375 ug/ml, 0.50 ug/ml, and 0.75 ug/ml. The cell viability was then assessed using the CCK-8 assay kit (CA1210, Cell Counting Kit-8, Dojindo Laboratories). After 48 h of treatment, the cells were incubated with the CCK-8 reagent for 2 h, and the absorbance values were measured using a microplate reader (BioTek Instruments) to evaluate cell viability (53).

Scratch assay

The migration capability of GCSCs was examined using a scratch assay. The cells were seeded at a density of 5×10^5 cells per well in a 6-well plate. Once the cells reached 90% confluence, a 200 μl pipette tip was used to create a scratch on the cell monolayer. The original medium was then replaced with RPMI1640 medium without fetal bovine serum to slow down cell proliferation. The healing of the scratch was monitored at specific time intervals using an inverted microscope (Olympus Corporation) to evaluate the migration capability (54).

Transwell assay

A total of 2×10^4 NC-KO and HNRNPA2B1-KO MKN-45 GCSCs or TMK-1 GCSCs were cultured in a 96-well Transwell system (3382, Corning Incorporated, USA) to assess cell invasion ability. Matrigel (356,234, Solarbio) was pre-coated inside the upper chamber of the Transwell system. An untreated GC stem cell suspension was seeded into the upper chamber, and RPMI-1640 medium containing 20% FBS was added to the lower chamber as a chemoattractant. After 24 h, cells on the upper surface of the polycarbonate membrane were removed using cotton swabs, while the cells on the lower side were fixed with 100% methanol. The fixed cells were stained with crystal violet (114359, Sigma-Aldrich, USA), and the number of cells that penetrated the membrane was counted under a microscope (54).

Sphere formation experiments

GCSCs derived from MKN-45 and TMK-1 cells in good condition were digested, centrifuged, and collected, followed by two PBS washes. Cells were counted, and 5×10^4 cells per well were seeded into ultra-low attachment 6-well plates (3471, Corning Incorporated, USA). Cells were cultured in a tumor stem cell sphere formation medium (P2401, Shanghai Qida Biological) for 14 days, after which the number of visible spheres was counted (55, 56).

TUNEL assay

Cells treated with 5-FU (F6627, Sigma-Aldrich, USA) were fixed with 4% paraformaldehyde and permeabilized with 0.5% Triton-X 100. Cells were then stained using an *in situ* cell death detection kit (Roche) following the manufacturer's protocol. DNA fragmentation was observed using the TUNEL assay. Fluorescence images were obtained using a confocal microscope (Carl Zeiss) (50).

Measurement of resting OCR

To evaluate mitochondrial oxidative phosphorylation efficiency, OCR was measured using the XF96 Extracellular Flux Analyzer (Seahorse Bioscience, USA). 2×10^4 NC-KO and HNRNPA2B1-KO MKN-45 GCSCs or TMK-1 GCSCs were seeded into a 96-well microplate. Cells were cultured in RPMI-1640 medium containing 10% fetal bovine serum. Prior to measurement, cells were equilibrated for 1 h in serum-free, CO_2-free conditions, and then OCR readings were taken (57).

Measurement of ECAR

ECAR was measured using the XF96 Extracellular Flux Analyzer to assess glycolysis levels in cells. 2×10^4 NC-KO and HNRNPA2B1-KO MKN-45 GCSCs or TMK-1 GCSCs were seeded into a 96-well plate. Cells were pre-treated as in OCR measurements, and glycolysis pathway-related drugs were injected following protocol to ensure accurate ECAR measurements (57).

JC-1 staining for mitochondrial membrane potential

The JC-1 dye (M34152, Thermo Fisher Scientific) was used to stain mitochondrial membrane potential following the manufacturer's protocol. 5×10^5 NC-KO and HNRNPA2B1-KO MKN-45 GCSCs or TMK-1 GCSCs were collected, stained with JC-1, and analyzed using a flow cytometer (BD Biosciences, USA) to evaluate mitochondrial membrane potential changes based on red/green fluorescence (58).

Detection of cellular reactive oxygen species (ROS) levels by DCFDA assay

5×10^5 NC-KO and HNRNPA2B1-KO MKN-45 GCSCs or TMK-1 GCSCs were incubated at 37 °C with fresh culture

medium containing 10 μM DCFH-DA (D6883, Sigma-Aldrich) for 30 min. After three PBS washes, cells were lysed in lysis buffer (50% methanol in 0.1 M NaOH). The supernatant was collected after cells were scraped from the plate and centrifuged at 4500 rpm for 5 min. Fluorescence was measured at 488/525 nm using a Synergy H1 multimode reader (Biotek). Data were normalized to protein concentration (59).

In vivo *validation*

Female BALB/c nude mice aged 4 to 6 weeks were obtained from the Nanjing Biomedical Research Institute (Nanjing, China). Mice were housed under pathogen-free conditions. Tumor cells (1×10^6 cells/100 μl PBS) were injected subcutaneously into one thigh of each mouse (8 mice per group). Tumor volume was measured every 3 days. When tumors reached 100 mm^3, 5-FU (20 mg/kg) or saline was administered intraperitoneally. After 4 weeks, mice were euthanized, and subcutaneous tumor tissues were fixed in 4% paraformaldehyde and embedded in paraffin. Tumor volume and weight were monitored, and growth curves were plotted. Tumor tissue was analyzed using flow cytometry ($CD24^+CD44^+$), and Ki-67 and cleaved Caspase-3 were used as markers for proliferation and apoptosis, respectively, in immunohistochemical analysis (60).

IHC

After animal experiments, lung tissue sections were prepared and immunohistochemically stained. Paraffin-embedded sections were deparaffinized, antigens were retrieved, and endogenous peroxidase activity was blocked with 3% hydrogen peroxide. Non-specific staining was reduced using goat serum. Rabbit anti-Caspase-3 (1:100, ab32351, Abcam) and rabbit anti-Ki67 (1:500, ab15580, Abcam) primary antibodies were applied overnight at 4 °C. The following day, sections were incubated with anti-rabbit IgG polymer (PV-6000, Beijing Zhongshan Golden Bridge Biotechnology), stained with DAB for 3 min, counterstained with hematoxylin, dehydrated, and sealed with neutral resin. Protein expression was semi-quantified by multiplying staining intensity and stained area scores. Five random fields were selected and observed under a microscope (Nikon, Tokyo, Japan) (61–63).

Transmission electron microscopy (TEM)

A TalosTM F200X S/TEM transmission electron microscope (Thermo Scientific) was used to observe changes in cellular morphology. The cells were fixed in a phosphate buffer solution containing 2.5% glutaraldehyde, followed by dehydration and embedding. Staining of the samples was performed using uranyl acetate and lead citrate to enhance image contrast. TEM was employed to observe and record any abnormalities in the number, size, and structure of mitochondria (64).

Statistical analysis

All data were derived from at least three independent experiments and presented as mean ± standard deviation (SD). Two independent samples *t* test was used for the comparison between the two groups. One-way analysis of variance (ANOVA) followed by Tukey's HSD *post hoc* test was performed for comparisons among three or more groups if the variance analysis indicated significant differences. For non-normal distribution or unequal variances, the Mann-Whitney U test or Kruskal-Wallis H test was utilized. Statistical analyses were conducted using GraphPad Prism 9 (GraphPad Software, Inc.) and R language. The significance level for all tests was set at 0.05, and *p*-values less than 0.05 (two-tailed) were considered statistically significant.

Ethics approval and consent to participate

All animal experiments were conducted under the approval of the institutional animal ethical committee of the Third Bethune Hospital of Jilin University and in compliance with the ARRIVE guidelines.

Data availability

All data generated or analyzed during this study are included in this article.

Supporting information—This article contains supporting Information.

Author contributions—S. C. and B. F. formal analysis; S. C. investigation; S. C. writing–original draft;; B. F. data curation; B. F. writing–review and editing. M. Y. supervision, M. Y. funding acquisition; S. C., B. F., and M.Y. conceptualization.

Conflict of interest—The authors declare that they have no conflicts of interest with the contents of this article.

Abbreviations—The abbreviations used are: DEGs, differentially expressed genes; ECAR, extracellular acidification rate; GC, Gastric cancer; GCSCs, gastric cancer stem cells; GEO, gene expression omnibus; hnRNPs, heterogeneous nuclear ribonucleoproteins; HPA, human protein atlas; IHC, immunohistochemistry; OCR, oxygen consumption rate; TCGA, tumor cancer genome atlas.

References

1. Pan, G., Liu, Y., Shang, L., Zhou, F., and Yang, S. (2021) EMT-associated microRNAs and their roles in cancer stemness and drug resistance. *Cancer Commun.* **41**, 199–217
2. Rao, X., Zhang, C., Luo, H., Zhang, J., Zhuang, Z., Liang, Z., *et al.* (2022) Targeting gastric cancer stem cells to enhance treatment response. *Cells* **11**, 2828
3. Zhong, T., Zhang, W., Guo, H., Pan, X., Chen, X., He, Q., *et al.* (2022) The regulatory and modulatory roles of TRP family channels in malignant tumors and relevant therapeutic strategies. *Acta Pharmaceutica Sinica B* **12**, 1761–1780
4. Norwood, D. A., Montalvan-Sanchez, E., Dominguez, R. L., and Morgan, D. R. (2022) Gastric cancer. *Gastroenterol. Clin. North America* **51**, 501–518
5. Thrift, A. P., Wenker, T. N., and El-Serag, H. B. (2023) Global burden of gastric cancer: epidemiological trends, risk factors, screening and prevention. *Nat. Rev. Clin. Oncol.* **20**, 338–349

6. Qi, J., Li, M., Wang, L., Hu, Y., Liu, W., Long, Z., *et al.* (2023) National and subnational trends in cancer burden in China, 2005–20: an analysis of national mortality surveillance data. *The Lancet Public Health* **8**, e943–e955
7. Otaegi-Ugartemendia, M., Matheu, A., and Carrasco-Garcia, E. (2022) Impact of cancer stem cells on therapy resistance in gastric cancer. *Cancers* **14**, 1457
8. Vasefifar, P., Motafakkerazad, R., Maleki, L. A., Najafi, S., Ghrobani-nezhad, F., Najafzadeh, B., *et al.* (2022) Nanog, as a key cancer stem cell marker in tumor progression. *Gene* **827**, 146448
9. Jiang, X., Liu, B., Nie, Z., Duan, L., Xiong, Q., Jin, Z., *et al.* (2021) The role of m6A modification in the biological functions and diseases. *Sig. Transduct. Target Ther.* **6**, 74
10. Glinos, D. A., Garborcauskas, G., Hoffman, P., Ehsan, N., Jiang, L., Gokden, A., *et al.* (2022) Transcriptome variation in human tissues revealed by long-read sequencing. *Nature* **608**, 353–359
11. Wang, X., Li, J., Bian, X., Wu, C., Hua, J., Chang, S., *et al.* (2021) CircURI1 interacts with hnRNPM to inhibit metastasis by modulating alternative splicing in gastric cancer. *Proc. Natl. Acad. Sci. U. S. A.* **118**, e2012881118
12. Su, R., Fan, L.-H., Cao, C., Wang, L., Du, Z., Cai, Z., *et al.* (2021) Global profiling of RNA-binding protein target sites by LACE-seq. *Nat. Cell Biol.* **23**, 664–675
13. Meng, Y., Zhao, Q., An, L., Jiao, S., Li, R., Sang, Y., *et al.* (2021) A TNFR2–hnRNPK Axis promotes primary liver cancer development via activation of YAP signaling in hepatic progenitor cells. *Cancer Res.* **81**, 3036–3050
14. Wang, X., Wang, J., Tsui, Y.-M., Shi, C., Wang, Y., Zhang, X., *et al.* (2021) RALYL increases hepatocellular carcinoma stemness by sustaining the mRNA stability of TGF-β2. *Nat. Commun.* **12**, 1518
15. Xia, Y., Lv, J., Jiang, T., Li, B., Li, Y., He, Z., *et al.* (2021) CircFAM73A promotes the cancer stem cell-like properties of gastric cancer through the miR-490-3p/HMGA2 positive feedback loop and HNRNPK-mediated β-catenin stabilization. *J. Exp. Clin. Cancer Res.* **40**, 103
16. Yang, Y., Wei, Q., Tang, Y., Yuanyuan, W., Luo, Q., Zhao, H., *et al.* (2020) Loss of hnRNPA2B1 inhibits malignant capability and promotes apoptosis via down-regulating Lin28B expression in ovarian cancer. *Cancer Lett.* **475**, 43–52
17. Yao, S., Yin, X., Chen, T., Chen, W., Zuo, H., Bi, Z., *et al.* (2021) ALDH2 is a prognostic biomarker and related with immune infiltrates in HCC. *Am. J. Cancer Res.* **11**, 5319–5337
18. Xiao, R., Wang, S., Guo, J., Liu, S., Ding, A., Wang, G., *et al.* (2022) Ferroptosis-related gene NOX4, CHAC1 and HIF1A are valid biomarkers for stomach adenocarcinoma. *J. Cell. Mol. Medi.* **26**, 1183–1193
19. Yu, Y., Wang, Z., Zheng, Q., and Li, J. (2021) FAM72 serves as a biomarker of poor prognosis in human lung adenocarcinoma. *Aging.* **13**, 8155–8176
20. Nandagopal, S., Choudhary, G., Sankanagoudar, S., Banerjee, M., Elhence, P., Jena, R., *et al.* (2024) Expression of stem cell markers as predictors of therapeutic response in metastatic prostate cancer patients. *Urol. Oncol. Semin. Original Invest.* **42**, 68.e21–68.e31
21. Torre, L. A., Bray, F., Siegel, R. L., Ferlay, J., Lortet-Tieulent, J., and Jemal, A. (2015) Global cancer statistics, 2012. *CA A. Cancer J. Clinicians* **65**, 87–108
22. Ferlay, J., Soerjomataram, I., Dikshit, R., Eser, S., Mathers, C., Rebelo, M., *et al.* (2014) Cancer incidence and mortality worldwide: sources, methods and major patterns in GLOBOCAN 2012. *Intl J. Cancer* **136**, E359–E386
23. Kinugasa, H., Nouso, K., Tanaka, T., Miyahara, K., Morimoto, Y., Dohi, C., *et al.* (2015) Droplet digital PCR measurement of HER2 in patients with gastric cancer. *Br. J. Cancer* **112**, 1652–1655
24. Dai, P., Wang, Q., Wang, W., Jing, R., Wang, W., Wang, F., *et al.* (2016) Unraveling molecular differences of gastric cancer by label-free quantitative proteomics analysis. *IJMS* **17**, 69
25. Peng, W., Zhao, J., Liu, X., Li, C., Si, S., and Ma, R. (2021) hnRNPA2B1 regulates the alternative splicing of BIRC5 to promote gastric cancer progression. *Cancer Cell Int.* **21**, 281
26. Chu, S., Fei, B., and Yu, M. (2023) Molecular mechanism of Circ_0088300–BOLL interaction regulating mitochondrial metabolic reprogramming and involved in gastric cancer growth and metastasis. *J. Proteome Res.* **22**, 3793–3810
27. Brandi, J., Cecconi, D., Cordani, M., Torrens-Mas, M., Pacchiana, R., Dalla Pozza, E., *et al.* (2016) The antioxidant uncoupling protein 2 stimulates hnRNPA2/B1, GLUT1 and PKM2 expression and sensitizes pancreas cancer cells to glycolysis inhibition. *Free Radic. Biol. Med.* **101**, 305–316
28. El-Hattab, A. W., Craigen, W. J., and Scaglia, F. (2017) Mitochondrial DNA maintenance defects. *Biochim. Biophys. Acta (BBA) - Mol. Basis Dis.* **1863**, 1539–1555
29. Song, Y., Wang, W., Wang, B., and Shi, Q. (2023) The protective mechanism of TFAM on mitochondrial DNA and its role in neurodegenerative diseases. *Mol. Neurobiol.* **61**, 4381–4390
30. Mondal, P., Gadad, S. S., Adhikari, S., Ramos, E. I., Sen, S., Prasad, P., *et al.* (2021) TCF19 and p53 regulate transcription of TIGAR and SCO2 in HCC for mitochondrial energy metabolism and stress adaptation. *FASEB J.* **35**, e21814
31. Zhang, J., Cai, H., Sun, L., Zhan, P., Chen, M., Zhang, F., *et al.* (2018) LGR5, a novel functional glioma stem cell marker, promotes EMT by activating the Wnt/β-catenin pathway and predicts poor survival of glioma patients. *J. Exp. Clin. Cancer Res.* **37**, 225
32. Ryskalin, L., Busceti, C. L., Biagioni, F., Limanaqi, F., Familiari, P., Frati, A., *et al.* (2019) Prion protein in glioblastoma multiforme. *IJMS* **20**, 5107
33. Hamzehlou, S., Momeny, M., Zandi, Z., Kashani, B., Yousefi, H., Dehpour, A. R., *et al.* (2019) Anti-tumor activity of neratinib, a pan-HER inhibitor, in gastric adenocarcinoma cells. *Eur. J. Pharmacol.* **863**, 172705
34. Min, Z., Zhu, Y., Hong, X., Yu, Z., Ye, M., Yuan, Q., *et al.* (2020) Synthesis and biological evaluations of monocarbonyl curcumin inspired pyrazole analogues as potential anti-colon cancer agent. *DDDT* **14**, 2517–2534
35. Hu, Z., Chen, G., Zhao, Y., Gao, H., Li, L., Yin, Y., *et al.* (2023) Exosome-derived circCCAR1 promotes CD8 + T-cell dysfunction and anti-PD1 resistance in hepatocellular carcinoma. *Mol. Cancer* **22**, 55
36. Pan, Z., Zhao, R., Li, B., Qi, Y., Qiu, W., Guo, Q., *et al.* (2022) EWSR1-induced circNEIL3 promotes glioma progression and exosome-mediated macrophage immunosuppressive polarization via stabilizing IGF2BP3. *Mol. Cancer* **21**, 16
37. Xuan, Y., Wang, J., Ban, L., Lu, J.-J., Yi, C., Li, Z., *et al.* (2015) hnRNPA2/B1 activates cyclooxygenase-2 and promotes tumor growth in human lung cancers. *Mol. Oncol.* **10**, 610–624
38. Hung, C.-Y., Wang, Y.-C., Chuang, J.-Y., Young, M.-J., Liaw, H., Chang, W.-C., *et al.* (2017) Nm23-H1-stabilized hnRNPA2/B1 promotes internal ribosomal entry site (IRES)-mediated translation of Sp1 in the lung cancer progression. *Sci. Rep.* **7**, 9166
39. Qing, X., Jiang, J., Yuan, C., Xie, K., and Wang, K. (2023) Expression patterns and immunological characterization of PANoptosis -related genes in gastric cancer. *Front. Endocrinol.* **14**, 1222072
40. Troemel, E. R., Chu, S. W., Reinke, V., Lee, S. S., Ausubel, F. M., and Kim, D. H. (2006) p38 MAPK regulates expression of immune response genes and contributes to longevity in C. elegans. *PLoS Genet.* **2**, e183
41. Ramírez-Vélez, R., García-Hermoso, A., Correa-Rodríguez, M., Fernández-Irigoyen, J., Palomino-Echeverría, S., Santamaría, E., *et al.* (2022) Effects of different doses of exercise on inflammation markers among adolescents with overweight/obesity: HEPAFIT study. *J. Clin. Endocrinol. Metab.* **107**, e2619–e2627
42. Deng, Y.-J., Ren, E.-H., Yuan, W.-H., Zhang, G.-Z., Wu, Z.-L., and Xie, Q.-Q. (2020) GRB10 and E2F3 as diagnostic markers of osteoarthritis and their correlation with immune infiltration. *Diagnostics* **10**, 171
43. Peng, X., Wang, Y., Hu, H., Zhang, X., and Li, Q. (2019) Identification of the molecular subgroups in coronary artery disease by gene expression profiles. *J. Cell Physiol.* **234**, 16540–16548
44. Rao, Y., Zhu, J., Zheng, H., Dong, W., and Lin, Q. (2022) A novel melanoma prognostic model based on the ferroptosis-related long non-coding RNA. *Front. Oncol.* **12**, 929960
45. Wei, L., Chang, J., Han, Z., Wang, R., and Song, L. (2019) Recombinant human growth hormone (rhGH) treatment of MKN-45 xenograft mice improves nutrition status and strengthens immune function without promoting tumor growth. *PLoS One* **14**, e0210613

46. Zhang, C., Li, C., He, F., Cai, Y., and Yang, H. (2011) Identification of CD44+CD24+ gastric cancer stem cells. *J. Cancer Res. Clin. Oncol.* **137**, 1679–1686
47. Gómez-Gallegos, A. A., Ramírez-Vidal, L., Becerril-Rico, J., Pérez-Islas, E., Hernandez-Peralta, Z. J., Toledo-Guzmán, M. E., *et al.* (2023) CD24+CD44+CD54+EpCAM+ gastric cancer stem cells predict tumor progression and metastasis: clinical and experimental evidence. *Stem Cell Res. Ther.* **14**, 16
48. Zhang, Y., Yang, L., Dai, G., and Cao, H. (2018) Knockdown of PHGDH potentiates 5-FU cytotoxicity in gastric cancer cells via the Bcl-2/Bax/caspase-3 signaling pathway. *Int. J. Clin. Exp. Pathol.* **11**, 5869–5876
49. Gupta, A., Yadav, S., PT, A., Mishra, J., Samaiya, A., Panday, R. K., *et al.* (2020) The HNRNPA2B1–MST1R–Akt axis contributes to epithelial-to-mesenchymal transition in head and neck cancer. *Lab. Invest.* **100**, 1589–1601
50. Jo, M. J., Jeong, S., Yun, H. K., Kim, D. Y., Kim, B. R., Kim, J. L., *et al.* (2019) Genipin induces mitochondrial dysfunction and apoptosis via downregulation of Stat3/mcl-1 pathway in gastric cancer. *BMC Cancer* **19**, 739
51. Zang, S., Yin, X., and Li, P. (2023) FTO-mediated m6A demethylation regulates GnRH expression in the hypothalamus via the PLCβ3/Ca2+/CAMK signalling pathway. *Commun. Biol.* **6**, 1297
52. Wang, Y., Li, J., Du, C., Zhang, L., Zhang, Y., Zhang, J., *et al.* (2019) Upregulated circular RNA circ-UBE2D2 predicts poor prognosis and promotes breast cancer progression by sponging miR-1236 and miR-1287. *Translational Oncol.* **12**, 1305–1313
53. Terzioğlu, G., Türksoy, Ö., and Bayrak, Ö. F. (2018) Identification of an mtDNA setpoint associated with highest levels of CD44 positivity and chemoresistance in HGC-27 and MKN-45 gastric cancer cell lines. *Cell J. (Yakhteh)* **20**, 312–317
54. Ma, C., Wang, X., Yang, F., Zang, Y., Liu, J., Wang, X., *et al.* (2020) Circular RNA hsa_circ_0004872 inhibits gastric cancer progression via the miR-224/Smad4/ADAR1 successive regulatory circuit. *Mol. Cancer* **19**, 157
55. Sun, J., Sun, B., Zhu, D., Zhao, X., Zhang, Y., Dong, X., *et al.* (2017) HMGA2 regulates CD44 expression to promote gastric cancer cell motility and sphere formation. *Am. J. Cancer Res.* **7**, 260–274
56. Bagheri, V., Esmaeili, S.-A., Gholamin, M., and Abbaszadegan, M. R. (2022) Rapid isolation of gastric adenocarcinoma cancer stem cells as a target for autologous dendritic cell-based immunotherapy. *Iranian J. Biotechnol.* **20**, 38–46
57. Wang, L., Chai, X., Wan, R., Zhang, H., Zhou, C., Xiang, L., *et al.* (2020) Retracted: disulfiram chelated with copper inhibits the growth of gastric cancer cells by modulating stress response and wnt/β-catenin signaling. *Front. Oncol.* **14**, 1475033
58. Youn, D. H., Kim, N., Lee, A., Han, S. W., Kim, J.-T., Hong, E. P., *et al.* (2023) Autophagy and mitophagy-related extracellular mitochondrial dysfunction of cerebrospinal fluid cells in patients with hemorrhagic moyamoya disease. *Sci. Rep.* **13**, 13753
59. Hao, H., Cao, L., Jiang, C., Che, Y., Zhang, S., Takahashi, S., *et al.* (2017) Farnesoid X receptor regulation of the NLRP3 inflammasome underlies cholestasis-associated sepsis. *Cell Metab.* **25**, 856–867.e5
60. Zheng, Y., Dai, M., Dong, Y., Yu, H., Liu, T., Feng, X., *et al.* (2022) ZEB2/TWIST1/PRMT5/NuRD multicomplex contributes to the epigenetic regulation of EMT and metastasis in colorectal carcinoma. *Cancers* **14**, 3426
61. Zhou, X., Liang, T., Deng, J., Ng, K., Li, M., Lv, C., *et al.* (2021) Differential and prognostic significance of HOXB7 in gliomas. *Front. Cell Dev. Biol.* **9**, 697086
62. Liu, T., Yang, K., Chen, J., Qi, L., Zhou, X., and Wang, P. (2023) Comprehensive pan-cancer analysis of KIF18A as a marker for prognosis and immunity. *Biomolecules* **13**, 326
63. Sheehan, P. W., Nadarajah, C. J., Kanan, M. F., Patterson, J. N., Novotny, B., Lawrence, J. H., *et al.* (2023) An astrocyte BMAL1-BAG3 axis protects against alpha-synuclein and tau pathology. *Neuron* **111**, 2383–2398.e7
64. Minhas, P. S., Latif-Hernandez, A., McReynolds, M. R., Durairaj, A. S., Wang, Q., Rubin, A., *et al.* (2021) Restoring metabolism of myeloid cells reverses cognitive decline in ageing. *Nature* **590**, 122–128